Intracellular lipopolysaccharide regulates ER remodeling upon bacterial infection

Authors

Yi-Lin Cheng[1,2,3,*], João Mello-Vieira[1,2], Adriana Covarrubias-Pinto[1], Alexis Gonzalez[1], Santosh Kumar Kuncha[1,2,4], Chun Kew[1,2], Kaiyi Zhang[5], Muhammad Awais Afzal[6], Nour Diab[5], Sophia Borchert[7], Wenbo Chen[1,2], Timothy Chun Huang[3,8], Mathias Walter Hornef[5], Christian A. Hübner[6], Michael Hensel[7], Ivan Dikic[1,2,9,10,11,*]

[1]Institute of Biochemistry II, Faculty of Medicine, Goethe University, Frankfurt, Germany

[2]Buchmann Institute for Molecular Life Sciences, Goethe University, Frankfurt, Germany

[3]Institute of Basic Medical Sciences, College of Medicine, National Cheng Kung University, Tainan, Taiwan

[4]Altos Labs Inc, Bay Area Institute, Redwood City, CA, USA

[5]Institute of Medical Microbiology, RWTH University Hospital, Aachen, Germany

[6] Institute of Human Genetics, Jena University Hospital, Friedrich Schiller University, Jena, Germany

[7]Abt. Mikrobiologie, Universität Osnabrück, Osnabrück, Germany.

[8]School of Medicine, College of Medicine, National Cheng Kung University, Tainan, Taiwan

[9]Max Planck Institute of Biophysics, Frankfurt, Germany

[10]Fraunhofer Institute for Molecular Biology and Applied Ecology (IME),

[11]Lead contact

*Correspondence: dikic@biochem2.uni-frankfurt.de;
yilincheng@gs.ncku.edu.tw

Graphical Abstract

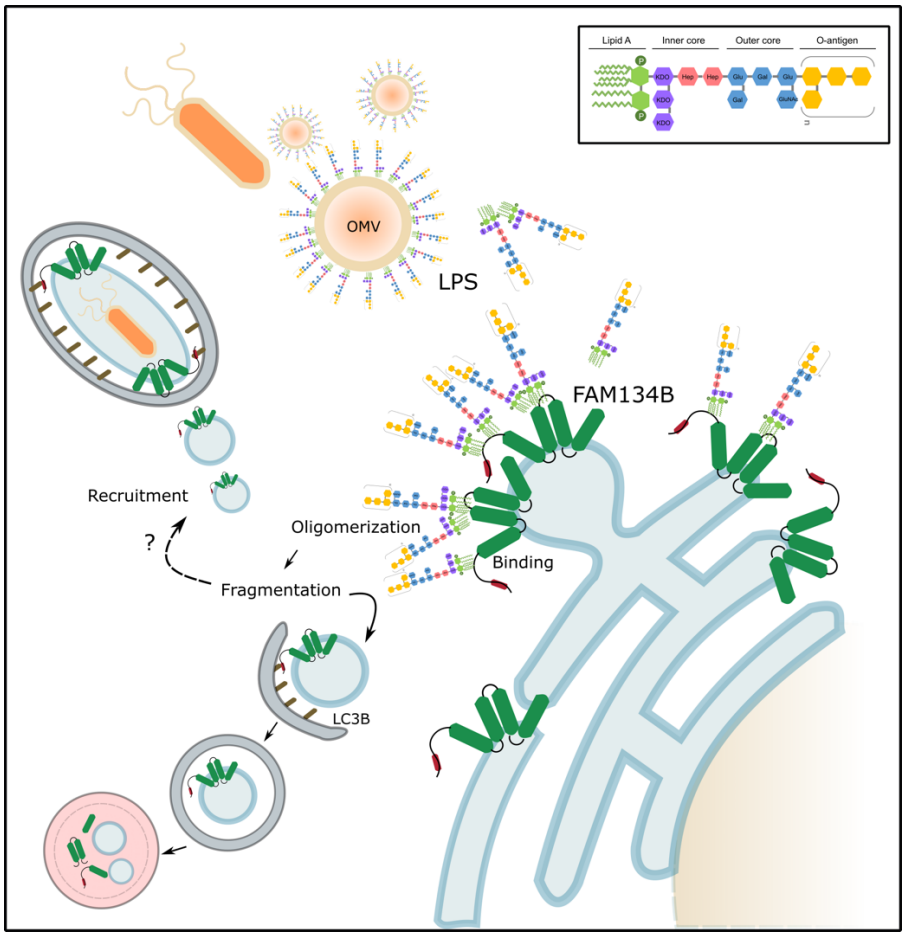

In Brief

Cytosolic LPS binds to the ER-phagy receptor FAM134B, triggering ER fragmentation, and subsequently, the formation of FAM134B-positive vacuoles for bacterial survival.

Highlights

- Intracellular LPS induces FAM134B-mediated ER fragmentation.
- Lipid A of LPS binds to FAM134B.
- O-antigen of LPS triggers oligomerization of FAM134B and membrane fragmentation.
- FAM134B-positive *Salmonella*-containing vacuoles are not acidified, providing a niche for *Salmonella* survival.
- Outer membrane vesicles are required for cytosolic LPS delivery to activate FAM134B-mediated ER fragmentation.

SUMMARY

The remodeling of endoplasmic reticulum (ER) is finely regulated by selective autophagy, known as ER-phagy. However, whether Gram-negative bacteria, which are known to manipulate the host membranous system, regulate ER-phagy remains elusive. We find that bacterial lipopolysaccharide (LPS) released upon infection with *Salmonella* Typhimurium colocalizes with FAM134B, a reticulon-like protein that operates as an ER-phagy receptor. Pulldown assays reveal that LPS binds directly to FAM134B. The interaction occurs via lipid A of LPS and positively charged amino acid residues on the amphipathic helices and C-terminal region of FAM134B. Upon binding, O-Antigen of LPS promotes FAM134B oligomerization and ER fragmentation in *in vitro* liposome membrane remodeling assays. Delivery of LPS into the cytoplasm via transfection significantly increases the number of FAM134B–LC3B-decorated ER fragments, which are recruited to *Salmonella*-containing vacuoles. Both intracellular and extracellular bacteria use outer membrane vesicles (OMVs) to deliver LPS into the cytosol for FAM134B activation and ER fragmentation. Taken together, our results show that Gram-negative bacteria subvert the host ER remodeling system to create bacteria-containing vacuoles that provide a niche for bacterial survival.

INTRODUCTION

Multiple intracellular Gram-negative bacteria have been identified to manipulate host membrane system, including the endoplasmic reticulum (ER), which is the most abundant membranous system in the mammalian cells, to create a niche for bacteria survival (Escoll et al., 2016). However, whether there is a common component of Gram-negative bacteria participating in the regulation of ER membranes is unclear. The selective autophagy of the ER (ER-phagy) has recently been identified as the master mechanism for ER remodeling and turnover (Gubas and Dikic, 2022), enabling lysosomal degradation of different ER components, which are engulfed into autophagosomes through the interaction of LC3B with ER-phagy receptors (Chino and Mizushima, 2020; Gubas and Dikic, 2022). Eight mammalian ER-phagy receptors have been identified, including the FAM134 family (Khaminets et al., 2015; Kumar et al., 2021; Reggio et al., 2021), RTN3 (Grumati et al., 2017), Sec62 (Fumagalli et al., 2016), CCPG1 (Smith et al., 2018), ATL3 (Chen et al., 2019), TEX264 (An et al., 2019; Chino et al., 2019), and CALCOCO1(Nthiga et al., 2020), which facilitate the degradation of different ER subdomains and respond to different types of stress conditions. The FAM134 family and RTN3L, in particular, are able to induce significant ER remodeling. They contain two hairpin-like domains (transmembrane domains; TM) anchored into the lipid bilayer and connected by an amphipathic helix (AH) linker, as well as another carboxy-terminal AH, which is connected to the second TM. Together they form a so-

81 called reticulum homology domain (RHD), whose integrity appears critical for ER-
82 phagy (Bhaskara et al., 2019; Grumati *et al.*, 2017; Khaminets *et al.*, 2015). The RHD
83 of FAM134B, the best-studied ER-phagy receptor, can sense highly positive
84 membrane curvature, thereby triggering the formation of FAM134B clusters that
85 provide an additional force for ER membrane budding and scission (Bhaskara *et al.*,
86 2019; Gonzalez et al., 2023; Jiang et al., 2020; Siggel et al., 2021).
87 LPS is the main component of the outer membrane of Gram-negative bacteria. It
88 is composed of a conserved lipid A moiety, the inner core and outer core
89 oligosaccharides, and O-antigen (O-Ag), the outermost part composed of a variable
90 number of repeating sugar residues. In recent decades, most studies have focused on
91 the extracellular role of LPS, which is specifically sensed on the plasma membrane by
92 the Toll-like receptor 4 (TLR4)/myeloid differentiation factor 2 (MD2) co-receptor
93 complex, that acts in conjugation with CD14 to trigger signaling cascades for the
94 expression of inflammatory genes (Park et al., 2009). The release of LPS by
95 intracellular *Salmonella* to cytosolic vesicles was reported by Portillo and colleagues
96 as early as 1997, however the targeted proteins and downstream effects are still
97 elusive (Garcia-del Portillo et al., 1997). More recently, human caspase-4 (mouse
98 homologue caspase-11) and caspase-5 have been identified as innate immune
99 receptors that specifically recognize intracellular LPS (Shi et al., 2014). The lipid A
100 moiety of LPS directly binds to the amino (N)-terminal caspase-activation and
101 recruitment domain (CARD) of these caspases, triggering their oligomerization and
102 activation (Shi *et al.*, 2014). Activated caspase-4/-11 further cleave gasdermin D to
103 liberate its N-terminal domain, which has membrane-pore-forming activity at the
104 plasma membrane and thereby induces pyroptosis (Aglietti et al., 2016; Ding et al.,
105 2016). Moreover, LPS on cytosolic *Salmonella* is also recognized by guanylate-binding
106 protein (GBP) 1, which initiates the assembly of a GBP coat for caspase-4 recruitment
107 and activation to trigger non-canonical inflammasome signaling (Santos et al., 2020).
108 Not only intracellular Gram-negative bacteria – after their escape from vacuoles -
109 expose LPS to the cytosol, but also extracellular Gram-negative bacteria by having
110 their LPS-enriched outer membrane vesicles (OMVs) internalized into the cell (Vanaja
111 et al., 2016). OMVs bud from Gram-negative bacterial cell envelopes and have a
112 diameter of 20 nm to 250 nm. The bacterial envelop is composed of the cytoplasmic
113 membrane and the outer membrane, which enclose the periplasmic space containing
114 a peptidoglycan layer and periplasmic proteins that stabilize the membrane through
115 various crosslinks (Juodeikis and Carding, 2022; Schwechheimer and Kuehn, 2015;
116 Silhavy et al., 2010). Upon infection, environmental stress factors released by the host
117 disturb the stability of those crosslinks and increase OMV budding. OMVs are
118 internalized into the host cell via endocytosis, and LPS is released from early

119 endosomes into the cytosol, where it activates caspase-11 (Vanaja *et al.*, 2016) and
120 possibly exerts other effects.
121 Here we describe a novel function for intracellular LPS mediated by binding to
122 FAM134B ER-phagy receptor. Both *Salmonella* infection and LPS transfection induced
123 FAM134B-mediated ER fragmentation. *Salmonella* LPS colocalized with FAM134B as
124 determined by immunofluorescence experiments, and biochemical analysis showed
125 that lipid A of LPS directly bound to FAM134B via electrostatic forces. Although lipid A
126 was sufficient for FAM134B binding, oligomerization of FAM134B and the following
127 membrane fragmentation required the presence of O-Ag of LPS. A part of the
128 fragmented FAM134B-positive ER was recruited by bacteria to form the *Salmonella*-
129 containing vacuole. We also found that OMVs are responsible for the delivery of LPS
130 from both intracellular and extracellular bacteria into the cytosol. Taken together, this
131 study identified FAM134B as a new intracellular target of LPS, enabling ER membrane
132 remodeling and formation of the survival niche.
133
134 **RESULTS**
135
136 **LPS colocalizes with FAM134B and triggers FAM134B-mediated ER**
137 **fragmentation**
138 To investigate whether intracellular Gram-negative bacteria activate ER-phagy,
139 we analyzed the protein turnover of several ER-phagy receptors, including FAM134B,
140 CCPG1, Sec62, RTN3L, and TEX264, during *Salmonella enterica* serovar
141 Typhimurium SL1344 infection (Figure S1A). The expression of FAM134B increased
142 upon infection while there were no significant changes for other ER-phagy receptors
143 (Figures S1A). We observed a slight decrease in RTN3L but it did not colocalize with
144 LC3B after *Salmonella* infection (Figure S1B). This result implies that *Salmonella*
145 mainly affects FAM134B-mediated ER-phagy, which is usually associated with
146 transcriptional up-regulation of FAM134B (Chino and Mizushima, 2020). In HeLa TREx
147 FLAG-HA-FAM134B-inducible cells, *Salmonella* strongly induced colocalization of
148 FAM134B puncta with LC3B puncta, indicating induction of FAM134B-mediated ER
149 fragmentation upon infection (Figure 1A). To our surprise, we found LPS puncta
150 (arrowheads) colocalizing with FAM134B which was not associated with bacteria
151 (arrows), indicated by nucleic acid staining with 4',6-diamidino-2-phenylindole (DAPI),
152 either in wild-type (WT) FAM134B or LC3B-interacting region mutant (mtLIR)
153 FAM134B (Figures 1A and S1C). Moreover, endogenous FAM134B, also colocalized
154 with *Salmonella* LPS after infection (Figure S1D). Quantitative analysis by confocal
155 quantitative image cytometer CQ1 showed that 40% of FAM134B puncta colocalized
156 with LPS after *Salmonella* infection (Figures 1B and 1C). The number of

157 FAM134B/LC3B-positive puncta after *Salmonella* infection was significantly increased
158 in WT FAM134B-expressing HeLa cells, but not in mtLIR FAM134B-expressing HeLa
159 cells, indicating *Salmonella* infection caused induction of FAM134B-mediated ER-
160 phagy and ER fragmentation (Figures 1D and S1E). Co-immunoprecipitation (Co-IP)
161 assays revealed that *Salmonella* enhanced interaction of FAM134B with LC3B-II in the
162 presence or absence of Bafilomycin A1 (BafA1) (Figure 1E). Our previous study
163 defined ER fragments as puncta containing FAM134B, LC3B-II and ER proteins that
164 do not directly bind LC3B (Gonzalez *et al.*, 2023). To clarify whether LPS can trigger
165 FAM134B-mediated ER fragmentation, we transfected *Salmonella* LPS in HeLa cells
166 followed by immunostaining and confocal microscopy analysis. The results showed
167 that LPS colocalized with FAM134B puncta and the number of FAM134B/LC3B-
168 positive puncta increased in presence of LPS (Figures 1 F and 1G). Moreover,
169 transfection of *Salmonella* LPS also triggered FAM134B fragments delivered to
170 lysosomes, indicating by LAMP1 (Figure S1F). Thus, *Salmonella* LPS initiated
171 FAM134B-mediated ER fragmentation.

172 **LPS binds to FAM134B via electrostatic force**

173 Since LPS colocalized with FAM134B in the confocal images, we hypothesized
174 that LPS binds directly to FAM134B. Therefore, we carried out a series of streptavidin
175 pull down assays to clarify the mode of interaction (Figure 2A). We used biotin-
176 conjugated *E. coli* O111:B4 LPS immobilized on streptavidin sepharose to study its
177 interaction with either HA-FAM134B or HA-RTN3L (Figure 2B). We detected that biotin-
178 LPS strongly pulled down HA-FAM134B in a dose-dependent manner, but not HA-
179 RTN3L (Figure 2B). The binding of LPS to FAM134B was LIR motif-independent
180 (Figure S2A). Pulldown assays after transfection of biotin-LPS into cells expressing
181 FLAG-HA-FAM134B or FLAG-HA-RTN3L showed similar results (Figure S2B).
182 Importantly, upon *Salmonella* infection in cells expressing FLAG-HA-FAM134B, LPS
183 was also able to interact with FAM134B (Figure 2C). No significant interaction between
184 RTN3L and LPS was detected upon *Salmonella* infection (Figure 2C). To further clarify
185 which segment of LPS is required for binding to FAM134B, we performed a competition
186 assay. WT LPS (also called smooth (S)-LPS), rough LPS, including Ra-LPS (LPS
187 without O-Ag) and Re-LPS (LPS containing lipid A and three 2-Keto-3-deoxy-octonate
188 (KDO)), and lipid A, were preincubated with lysates containing FLAG-HA-FAM134B,
189 followed by incubation with biotin-LPS-immobilized streptavidin sepharose. We
190 analyzed whether the preincubation with different LPS variants can block the binding
191 of biotin-LPS to FAM134B (Figures 2D and 2E). The results reveal that all kinds of LPS
192 significantly reduced the binding ability of biotin-LPS to FAM134B, except Muramyl
193 dipeptide (MDP), which is another component of the bacteria cell wall, demonstrating
194 that lipid A is sufficient for FAM134B binding (Figure 2E). Furthermore, polymyxin B, a

195 cationic peptide antibiotic, which interacts with lipid A via ionic and hydrophobic forces,
196 inhibited the binding of biotin-LPS to FAM134B in a dose-dependent manner (Figure
197 2F).

198 Next, we characterized how FAM134B binds to LPS. Since lipid A contains
199 multiple negatively charged groups (Adams et al., 2014), we hypothesized that the
200 interaction might occur through electrostatic forces. We analyzed each domain of
201 FAM134B and found that two cytoplasmic amphipathic helices, the linker and C-
202 terminal region of the amphipathic helices (AHL and AHC), and the C-terminal region
203 (Cterm), are highly solvent-accessible and enriched with positively charged residues,
204 including arginine (R) and lysine (K) (Figure 2G). According to this analysis, we
205 mutated R or K residues to glutamic acid (E) in these three FAM134B regions (Figure
206 2H). We then evaluated the interactions of these mutants with biotin-LPS. Each mutant
207 FAM134B construct showed significantly reduced binding to biotin-LPS, and binding
208 was completely abolished when mutations in all three regions were combined (Figure
209 2I). Transfection of FAM134B TRIPLEmt (mutations in all three regions) robustly
210 blocked colocalization of FAM134B with LPS and LC3B (Figures 2J and 2K). These
211 results were also confirmed by co-immunoprecipitation experiments in which
212 FAM134B TRIPLEmt-HA co-precipitated significantly less LPS and LC3B-II compared
213 to FAM134B WT-HA (Figure 2L). Moreover, *in vitro* streptavidin pulldown assays
214 showed that biotin-LPS pulled down FAM134C and FAM134B with similar efficiency
215 whereas FAM134A interacted significantly weaker (Figure S2C). This result could be
216 explained by the fact that FAM134B and FAM134C have a high sequence similarity,
217 from which the sequence of FAM134A clearly deviates (Figure S2D-S2F).

218 **FAM134B oligomerization is triggered by O-Ag of LPS**

219 Oligomerization of FAM134B is reported to drive ER membrane scission followed
220 by ER-phagy induction (Jiang *et al.*, 2020). Especially, caspases also undergo
221 oligomerization after binding with LPS (Shi *et al.*, 2014). We therefore hypothesized
222 that LPS binds to FAM134B to induce its oligomerization. S-protein-FLAG-streptavidin
223 binding peptide (SFB)-FAM134B was expressed and purified from HEK293T cells
224 followed by incubation with S-LPS or lipid A. In order to analyze oligomeric species of
225 FAM134B, we performed blue native PAGE, which enforces migration of native protein
226 complexes or oligomers based solely on their molecular weight (Wittig et al., 2006),
227 followed by immunoblotting with FLAG. S-LPS significantly increased the presence of
228 FAM134B oligomers of approximately 720 kDa (Figure 3A). To our surprise, lipid A did
229 not show a similar effect, although it played a major role in binding to FAM134B,
230 suggesting that O-Ag is indispensable for the oligomerization of FAM134B. To test this
231 idea, we infected HeLa cells expressing SFB-FAM134B with an isogenic set of

232 *Salmonella* mutant strains with defined defects in the O-antigen biosynthesis, including
233 the *rfbP* (O-antigen transferase) and *rfaL* (O-antigen ligase) mutant strains lacking O-
234 Ag, the *rfaG* (glucosyltransferase I) mutant strain lacking O-Ag and outer core, as well
235 as the *rfaH* (transcriptional activator) mutant strain with reduced polymeric O-Ag
236 (Figures 3B and 3C) (Zenk et al., 2009). After infection, SFB-FAM134B was purified
237 and blue native PAGE analysis was performed. The results showed that FAM134B
238 oligomers in the range of ~720 kDa to ~1048 kDa were significantly reduced after
239 infection with any of the O-Ag-defective strains compared to WT and complemented
240 strains (Figure 3B).
241 FAM134B clustering would further induce membrane curvature and remodeling
242 (Bhaskara *et al.*, 2019). To further prove that O-Ag regulates membrane remodeling
243 driven by FAM134B, we conducted a liposome-remodeling assay in which incubation
244 with purified FAM134B drives membrane fragmentation (Bhaskara *et al.*, 2019). We
245 first determined the suitable lipid-to-protein ratio (LPR) for the examination of the effect
246 of LPS on FAM134B-triggered membrane fragmentation (Figures S3A and S3B). LPR
247 40:1 triggered strong liposome remodeling, indicated by a significant reduction of the
248 liposome diameter compared to the control group of liposomes only (Empty). LPR
249 100:1 had a moderate effect, resulting in a slightly reduced liposome size (Figures S3A
250 and S3B). Thus, we used LPR 100:1 to study the action of LPS (Figures 3D-3G). S-
251 LPS significantly enhanced the membrane remodeling effect of FAM134B compared
252 to liposomes incubated with FAM134B alone in a dose-dependent manner (Figures 3D
253 and 3E). Notably, LPS alone did not change the size of liposomes compared to the
254 control sample, demonstrating that LPS cannot fragment membrane by itself, but
255 enhances the action of FAM134B on membranes (Figures 3D and 3E). Compared to
256 S-LPS, Ra-LPS and Re-LPS, which lack the O-Ag, had less pronounced effects on the
257 size of liposomes, i.e. on the ability of FAM134B to induce membrane fragmentation
258 (Figures 3F and 3G). To further verify the role of O-Ag in ER fragmentation in cells, we
259 performed co-localization analysis of HA-FAM134B and LC3B after infection of WT, the
260 isogenic mutant strains without O-Ag, and the two complemented strains of Δ*rfaL* and
261 Δ*rfaG* (Figures 3H and S3C). The number of FAM134B/LC3B-positive puncta was
262 significantly reduced upon infection with O-Ag mutant strains, Δ*rfbP,* Δ*rfaL,* Δ*rfaG,* and
263 Δ*rfaH* strains*,* in comparison to the WT strain. On contrary, complemented strains of
264 Δ*rfaL* and Δ*rfaG* induced a similar number of FAM134B/LC3B-positive puncta as the
265 WT strain (Figures 3H and S3C). The bacteria count per cell did not show significant
266 differences among the groups (Figure 3I and S3C). Compared to S-LPS, transfection
267 of Ra-LPS, Re-LPS, and lipid A, which are the LPS without O-Ag, did not increase the
268 number of HA-FAM134B/LC3B-positive puncta (Figures S3D and S3E). The other two
269 cell wall components of bacteria, Pam3CSK4 and MDP, did not affect puncta formation

270 (Figures S3D and S3E). These results demonstrated that O-Ag of LPS triggered
271 oligomerization of FAM134B and FAM134B-mediated membrane remodeling.
272
273 **FAM134B is recruited to *Salmonella*-containing vacuoles and promoted bacteria**
274 **growth**
275 To further investigate the fate and function of FAM134B after infection, we
276 measured the FAM134B-mediated ER-phagy flux by mCherry-EGFP-FAM134B WT or
277 LIR mutant-inducible HeLa cells after *Salmonella* infection for 2 hr and 4 hr (Figures
278 S4A and S4B). Owing to the instability of EGFP in acidified environment, only the red
279 fluorescence of mCherry would be detected when FAM134B is delivered to lysosomes
280 (Chino *et al.*, 2019; Jiang *et al.*, 2020; Khaminets *et al.*, 2015). *Salmonella* strongly
281 induced formation of red FAM134B puncta 4 hr post-infection in mCherry-eGFP-
282 FAM134B WT HeLa cells, but not in cells expressing the LIR mutant (Figures S4A and
283 S4B). Interestingly, FAM134B positive for both GFP and mCherry was recruited to
284 bacteria producing vacuoles (Figures S4A-1). In cells with highly proliferative bacteria,
285 which usually occur after bacteria escape from *Salmonella*-containing vacuoles (SCVs)
286 into cytosol, double-color FAM134B was also recruited to bacteria (Figure S4C). In
287 *Salmonella*-infected intestinal tissue sections of 5 days-old suckling mice, FAM134B
288 was also recruited to *Salmonella* (Figure S4D). These structures were positive for
289 calnexin and REEP5, as well (Figure S4E and S4F). Moreover, in FAM134B knockout
290 (KO) mouse bone-marrow-derived macrophages (BMDMs), ER-surrounded
291 *Salmonella* were significantly reduced compared to WT BMDMs (Figures S5A-S5C).
292 These results suggest that *Salmonella* sequesters FAM134B, possibly to recruit ER
293 membrane to the vacuole.
294 According to previous studies, invasive *Salmonella* can survive in the
295 endolysosomal membrane-derived SCVs or be cleared after sequestration in
296 xenophagosomes (LaRock et al., 2015; Madan et al., 2012; Perrin et al., 2004;
297 Ravenhill et al., 2019; Wild et al., 2011). We decided to study whether the FAM134B-
298 positive structures belong to one of these two compartments. We observed that
299 bacteria decorated with FAM134B-HA, colocalized with LC3B but not with the
300 endolysosomal marker LAMP1 (Figure 4A). Quantitative analysis indicated that around
301 50% LC3B-positive *Salmonella*-containing compartments were FAM134B-positive
302 after *Salmonella* infection for 2 hr, and around 40 % at 4 hr and 6 hr post-infection, but
303 very few LAMP1-positive SCVs were FAM134B-positive (Figure 4B). Indeed, almost
304 all FAM134B/LC3B-positive vacuoles were lysotracker-negative, indicating lack of
305 acidification of the compartment (Figures 4C and 4D). The xenophagosomes without
306 FAM134B expression showed to be either lysotracker-positive or -negative, which is
307 due to the different stages of autophagy flux (Figures 4C and 4D). Depletion of

308 FAM134B significantly increased the percentage of lysotracker-positive
309 xenophagosomes (Figures 4E and 4F). In the interactome of FAM134B during
310 *Salmonella* infection, we identified multiple bacterial factors, including outer membrane
311 proteins, slyB and ompA, STM1249, turfA, steA, as well as sopB, which was reported
312 to block lysosome fusion with SCVs (Bakowski et al., 2010) (Figures S6). Nevertheless,
313 whether these bacterial proteins contribute to FAM134B-mediated bacterial survival
314 requires further investigation. To confirm the role of FAM134B in bacterial growth, we
315 performed a plating assay to measure colony-forming units (CFU) in FAM134B-WT or
316 FAM134B-LIR mutant inducible cells after *Salmonella* infection. Induction of WT
317 FAM134B, but not LIR mutant FAM134B increased CFU compared to non-inducible
318 group (Figure 4G). Depletion of FAM134B either in FAM134B knockdown HeLa cells,
319 FAM134B KO mouse embryonic fibroblasts (MEFs), and FAM134B KO BMDMs
320 reduced *Salmonella* multiplication (Figures 4H, 4I, and S5C). These results indicate
321 that recruitment of FAM134B enables the formation of a compartment without
322 acidification leading to bacterial survival.
323
324 **OMVs are required for LPS delivery to induce FAM134B-mediated ER remodeling**
325 Transmission electron microscopy (TEM) studies revealed that LPS secreted by
326 *Salmonella* is presented on vesicular structures that resemble OMVs generated by
327 bacteria (Garcia-del Portillo *et al.*, 1997). OMVs, which are enriched in LPS on the
328 surface, are also responsible for delivery of LPS from extracellular bacteria to the host
329 cell cytosol via endocytosis (Vanaja *et al.*, 2016). Hence, we investigated whether OMV
330 production is required for FAM134B-mediated ER fragmentation. OMV production is
331 governed by various mechanisms that detach the outer membrane from the underlying
332 peptidoglycan and then allow outward budding to form vesicles (Juodeikis and Carding,
333 2022; Schwechheimer and Kuehn, 2015). For example, the outer membrane protein A
334 (OmpA) is the major outer membrane porin in *E. coli* and *S. enterica* and is linked to
335 peptidoglycan. Lack of OmpA results in decreased stability of the outer membrane and
336 increased release of OMVs, which has been previously reported for *S. enterica*
337 serovars Typhimurium (Deatherage et al., 2009) and Typhi (Nevermann et al., 2019),
338 and was confirmed for the mutant strains used in our study by ultrastructural analyses
339 (Figure S7). Another example is TolAB, which encodes components of the multi-
340 subunit Tol-Pal complex that controls the constriction of the cell envelope during cell
341 division. Mutant strains lacking TolAB show increased OMV production due to defects
342 in partitioning the outer membrane during cell elongation and septation (Szczepaniak
343 et al., 2020). DegS is also involved in OMV production. It is part of a sensor system
344 responding to periplasmic stress, which is, for example, induced by accumulation of
345 misfolded secretory proteins. If the stress response system is absent, the accumulation

346 of misfolded proteins in the periplasm induces increased OMV production to remove
347 toxic aggregates (Nevermann *et al.*, 2019). On the contrary, PagL is a deacylase that
348 removes one lipid from hexa- or hepta-acylated lipid A of LPS (Kawasaki et al., 2004).
349 This modification alters topology of LPS in the outer membrane, resulting in increased
350 membrane curvature and OMV release (Elhenawy et al., 2016). We therefore
351 established *Salmonella* strains mutated in the genes *pagL*, *ompA*, *tolAB*, and *degS,*
352 and obtained the images of OMVs production by scanning electron microscopy (SEM)
353 and TEM followed by measurement of OMVs amount and size distribution (Figure S7).
354 Compared to the WT strain, the Δ*ompA*, Δ*tolAB*, and Δ*degS* strains showed increased
355 production of OMVs. Conversely, no vesicles could be detected with the Δ*pagL* strain
356 (Figure S7C), which is in line with previous findings showing that deletion of *pagL*
357 results in decreased generation of OMVs by intracellular *Salmonella* (Elhenawy *et al.*,
358 2016).
359 Mutation of *ompA*, *tolAB*, and *degS*, associated with increased OMVs production,
360 augmented the number of FAM134B/LC3B-positive puncta to varying degrees (Figures
361 5A, 5B, and S7D). Especially, mutation of *tolAB* strongly increased puncta formation
362 compared to the WT group. Conversely, the number of FAM134B/LC3B-positive
363 puncta decreased when *pagL* was mutated (Figures 5A and S7D). The LPS levels in
364 the cell lysates and the amount of LPS interacting with FAM134B positively correlated
365 with the number of FAM134B/LC3B-positive puncta (Figures 5A and 5C). The bacterial
366 counts for the different isogenic mutant strains did not show significant change at 2 hr
367 post-infection (Figure 5B). To further explore whether OMVs can directly activate
368 FAM134B-mediated ER fragmentation, we purified OMVs from *Salmonella* and treated
369 HeLa TREx FLAG-HA-FAM134B cells with these OMVs. After treatment with
370 *Salmonella* OMVs, we observed colocalization of LPS and HA-FAM134B. The number
371 of FAM134B/LC3B-positive puncta also increased (Figures 5D and 5E). To differentiate
372 whether FAM134B mainly bound to shed LPS or the LPS on OMVs, we stained OMVs
373 by Vybrant DiO dye after purification and then treated the cells. Confocal microscopy
374 showed that FAM134B/LPS-positive puncta did not colocalize with Vybrant DiO-
375 positive OMVs (Figure S8A). Furthermore, the O-Ag mutant strains-derived OMVs lost
376 the ability to trigger FAM134B-mediated ER fragmentation (Figure 5F). We further
377 tested whether extracellular bacteria, more specifically Enteropathogenic *Escherichia*
378 *coli* (EPEC), can induce a similar phenomenon. In addition to direct exposure,
379 transwells with 0.45 μm polycarbonate membranes were used to prevent bacteria
380 passage but allow OMVs transition. The results reveal that EPEC induced similar
381 amount of FAM134B/LC3B-positive puncta in direct infection and transwell system
382 (Figures 5G and 5H). The *E. coli* strain without O-Ag, BL21, was used as the negative
383 control, showing no significant formation of FAM134B puncta (Figures 5I and S8B).

384 The number of LC3B-decorated FAM134B puncta also increased in the cells with
385 EPEC-derived OMVs, which were pre-stained by Vybrant DiO after purification.
386 However, BL21-derived OMVs did not cause same effect (Figures 5I and S8B). These
387 results suggest that intracellular and also extracellular bacteria utilize OMVs for the
388 delivery of LPS to activate FAM134B-mediated ER fragmentation.
389
390 **DISCUSSION**
391 Here we report that FAM134B, an ER-phagy receptor, interacts with LPS to induce
392 ER membrane fragmentation and to form vacuoles that surround *Salmonella* for
393 bacterial survival. The interaction between LPS and FAM134B was mainly mediated
394 by lipid A and positively charged amino acid residues in FAM134B. Besides, O-Ag of
395 LPS was responsible for oligomerization of FAM134B and the subsequent membrane
396 fragmentation, although it remains to be investigated how the molecular dynamics are
397 regulated in detail.
398 We have previously shown that the wedge-shaped membrane inclusions formed
399 by the RHD of FAM134B trigger membrane curvature followed by membrane
400 fragmentation (Bhaskara *et al.*, 2019). Our recent study (Gonzalez *et al.*, 2023)
401 uncovered that ubiquitination of the RHD domain finely regulates its membrane
402 remodeling ability, promotes large-scale membrane deformation, increases receptor
403 cluster size, and enhances ER-phagy flux. In the present study, we found that
404 mutations of multiple lysine residues of FAM134B, which are also sites for
405 ubiquitination, significantly inhibited the binding ability to LPS (Figure 2). Thus, LPS
406 might play a similar role as ubiquitination for FAM134B oligomer formation and
407 membrane fragmentation.
408 The fact that LPS can directly bind to FAM134B to induce ER membrane
409 fragmentation (Figure 3) and ER-phagy supports a model in which *Salmonella* hijacks
410 ER-phagy and prevents FAM134B-positive autophagosomes from traveling to
411 lysosomes. SopB, a *Salmonella* virulence factor that we found to bind to FAM134B,
412 could possibly play a role in this scenario as it inhibits autophagosome-lysosome
413 fusion so that the FAM134B-positive vacuoles cannot be acidified, allowing the
414 bacteria to multiply (Figures 4 and S6) (Bakowski *et al.*, 2010). However, this needs
415 to be investigated further. Based on the knockdown assay, we speculate that without
416 FAM134B, bacteria cannot sequester enough ER membrane, resulting in a vacuole
417 that is more susceptible to xenophagy. Recently, Gatica *et al.* showed that *Salmonella*
418 SopF inhibits amino acid starvation-induced FAM134B-mediated ER-phagy in
419 HEK293T cells, suggesting *Salmonella* effectors may play controversial roles in
420 different conditions. Nevertheless, this work did not test the role of SopF in
421 *Salmonella* or LPS-induced ER-phagy (Gatica et al., 2024).

422 In addition to vacuole formation, this mechanism may also serve other purposes,
423 since ER remodeling participates in different physiological functions, such as vesicular
424 trafficking, the unfolded protein response, ER-associated degradation, ER tubule
425 formation, ER-lysosome associated degradation, and ER-organelle contact-site
426 formation (Gubas and Dikic, 2022). ER shaping and remodeling enables human cells
427 to deal with ER stress, which is triggered by live Gram-positive bacteria through the
428 innate sensor stimulator of interferon genes (STING), while simultaneously inducing
429 autophagy (Moretti et al., 2017). Upon ER stress induction, ER proteins were found to
430 co-fractionate with LC3B, suggesting that ER-phagy is activated to balance ER stress
431 and maintain homeostasis (Moretti *et al.*, 2017). It will be interesting to further
432 investigate whether FAM134B-mediated ER-remodeling is involved in other
433 pathogenic or immune responses upon Gram-negative bacterial infection.
434 Our immunofluorescence experiments showed that the FAM134B puncta mainly
435 colocalized with LPS that was not localized on OMVs (Figure S8A). Although we cannot
436 yet draw any conclusions about the properties of the LPS released from OMVs, studies
437 on the binding between LPS and guanylate binding protein-1 (GBP1) provide us with
438 some clues for future investigations (Kutsch et al., 2020). GBP1 can bind directly to
439 lipid A moieties of LPS micelles, which form in aqueous solution (Santos et al., 2003),
440 or to LPS on the bacterial surface. It then undergoes polymerization, which is mediated
441 by the O-Ag (Kutsch *et al.*, 2020). Similarly, we found that binding of FAM134B to LPS
442 was mediated by lipid A moieties and O-Ag was required for oligomerization of
443 FAM134B. Moreover, FAM134B did not only bind to secreted LPS, which might be
444 present in micellar form, but was also recruited to bacteria, which mirrors the finding
445 for GBP1. Furthermore, we observed that LPS puncta appeared at a quite early stage
446 of infection, when only few bacteria were present. How these bacteria release LPS is
447 still unclear. Nevertheless, several studies have shown that GBPs and the immunity-
448 related GTPase family member B10 (IRGB10) may play a crucial role in the release of
449 LPS into the cytosol. GBPs were shown to be recruited to intracellular pathogens and
450 lyse the pathogen-containing vacuoles, resulting in the release of bacteria into the
451 cytosol and LPS being detectable therein (Meunier et al., 2014). GBPs further recruit
452 IRGB10 to the bacterial surface, disrupting the bacterial cell membrane and releasing
453 bacterial ligands, including LPS (Man et al., 2016). Although we found in this study that
454 the ability of different *Salmonella* isogenic mutant strains to produce OMVs correlates
455 with intracellular LPS levels (Figures 5A and 5D), the mechanism for release of LPS
456 from the intracellular OMVs remains unknown.
457 In summary, our work reveals a novel LPS-binding protein, FAM134B, which
458 undergoes oligomerization after binding to LPS, thereby triggering ER fragmentation.
459 The fragmented ER membranes are recruited to *Salmonella* to form the niche for

460 bacterial survival. Overall, this study provided new mechanistic insights into the
461 pathways by which Gram-negative bacteria induce ER-remodeling and establish its
462 proliferative niche.
463

464 **Acknowledgments**

465 We thank Prof. Dr. Volkhard A. J. Kempf at the Institute for Medical Microbiology and
466 Infection Control, Hospital of the Goethe University for the kind gift of the EPEC
467 O127:H6 strain. We thank the staff at the Quantitative Proteomics Unit at Goethe
468 University for support with mass spectrometry and the Frankfurt Center for Advanced
469 Microscopy (FCAM) for access to microscopes. This research is supported by the
470 Deutsche Forschungsgemeinschaft (DFG, German Research Foundation), project
471 number 259130777-SFB 1177, the European Union (ERC, ER-REMODEL,
472 101055213), the HMWK-funded cluster grant ENABLE, and grants from Else Kroener
473 Fresenius Stiftung and Dr. Rolf M. Schwiete Stiftung to ID. M.H. was supported by
474 the DFG by project P8 in SFB1557 and HE1964/23-1 in priority program SPP 2225
475 'Exit Strategies'. C.A.H. was supported by the DFG HU 800/14-1. Y.L.C. was
476 supported by funding through a National Science and Technology Council, project
477 NSTC 112-2320-B-006-012-MY2 and project 108-2917-I-564-021.

478 **Author contribution**

479 Conceptualization, Y.L.C. and I.D.; Methodology, Y.L.C., S.K.K., K.C., A.C-P, A.G.,
480 C.K., J.M.V., M.A.A., S.B., M.W.H.,C.A.H., M.H., N.D., and W.C.; Investigation,
481 Y.L.C., S.K.K., A.C-P, A.G., J.M.V., M.A.A., C.K. and K.C.; Writing – Y.L.C., S.K.K.,
482 K.C., A.C-P, A.G., C.K., M.W.H., M.H., T.C.W., C.A.H. and I.D.; Funding Acquisition,
483 I.D.; Resources, I.D., M.W.H., C.A.H. and M.H.; Supervision, I.D.

484 **Declaration of interests**

485 The authors declare no competing interests.

486 **Supplemental information**

487 Document S1. Figures S1–S8

488 **FIGURE LEGENDS**

489 **Figure 1. *Salmonella* LPS activates FAM134B-mediated ER fragmentation.**

490 (A) Immunofluorescence staining of HA, *Salmonella* LPS, and LC3B in HeLa TREx
491 inducible cell lines expressing FLAG-HA-FAM134B that were infected with SL1344 for

492 2 hr. DAPI staining was used for cell nuclear and bacteria DNA staining. Scale bar, 10
493 μm.

494 (B and C) Quantification of HA and *Salmonella* LPS staining in HeLa TREx inducible
495 cell lines expressing FLAG-HA-FAM134B infected with SL1344 for 2 hr. The number
496 of LPS-positive HA-FAM134B puncta per cell (B) and the percentage of LPS-positive
497 HA-FAM134B puncta in all HA-FAM134B puncta (C) were quantified using
498 CellPathfinder software.

499 (D) Number of LC3B-positive HA-FAM134B puncta in HeLa TREx inducible cell lines
500 expressing wild type (WT) or LIR mutant (mtLIR) FLAG-HA-FAM134B infected with
501 SL1344 for 2 hr. Representative images are shown in Figure S1C.

502 (E) Co-IP of endogenous LC3B-II with HA in HeLa TREx inducible cells without
503 doxycycline (Dox) treatment or with FLAG-HA-FAM134B WT or FLAG-HA-FAM134B
504 mtLIR after Dox treatment. The cells were infected with SL1344 for 2 hr and pretreated
505 with 200 ng/ml Bafilomycin A1 (BafA1) for 3 hr. GAPDH was used as an internal control
506 of input.

507 (F and G) Immunofluorescence staining and quantification of HA, *Salmonella* LPS, and
508 LC3B in HeLa TREx inducible cell lines expressing FLAG-HA-FAM134B transfected
509 with 1 μg/ml *Salmonella* LPS for 18 hr by lipofectamine 2000. Lipo, lipofectamine only.
510 (F) Arrows indicate the puncta with colocalization of HA-FAM134B and *Salmonella*
511 LPS, and arrowheads indicate the puncta with colocalization of HA-FAM134B and
512 LC3B. Scale bar, 10 μm. (G) Quantification of LC3B-positive HA-FAM134B puncta per
513 cell.

514 (B and C) Data presented as mean + standard error of the mean (sem), n=3, > 400
515 cells. Differences were statistically analyzed by an unpaired two-tailed Student's t-test

516 (D and G) Solid bars of boxes indicate the medians. Boxes represent interquartile
517 range from 25th to 75th percentile, and whiskers indicates 10th to 90th percentile.
518 Differences were statistically analyzed by one-way ANOVA and Tukey's multiple
519 comparison test. Data were collected 60 cells from three independent biological
520 replicates.

521 $^{**}p < 0.01$, $^{***}p < 0.001$. ns, not significant.

522

523 **Figure 2. LPS bind to FAM134B**

524 (A) Schematic representation of streptavidin pulldown assays.

525 (B) Streptavidin pulldown assays that determine the binding of the indicated amounts
526 of biotin-conjugated *E. coli* O111:B4 LPS and HA-tagged FAM134B or RTN3L in
527 FLAG-HA-FAM134B- or FLAG-HA-RTN3L-expressing HeLa TREx cell lysates.
528 GAPDH was used as an internal control of input.

529 (C) Co-IP of LPS with HA in HeLa TREx inducible cell lines without Dox treatment or
530 expressing FLAG-HA-FAM134B or FLAG-HA-RTN3L by Dox treatment, which were
531 infected with SL1344 for 2 hr. GAPDH was used as an internal control of input.

532 (D) Schematic representation of the LPS structure and the segments of different
533 mutant variants of LPS, including lipid A, Re-LPS, Ra-LPS, and smooth (S)-LPS. P,
534 phosphate; KDO, 3-deoxy-D-*manno*-octulosonic acid; Hep, L-*glycero*-D-*manno*-
535 heptose; PEtn, phosphatidyl-ethanolamine; Glc, D-glucose; Gal, D-galactose; GlcNac,
536 N-acetyl-D-glucosamine.

537 (E) Unlabeled S-LPS, Ra-LPS, Re-LPS, lipid A, and muramyl dipeptide (MDP) were
538 used for competition with the binding of biotin-conjugated *E. coli* O111:B4 LPS to HA-
539 tagged FAM134B in Dox-induced FLAG-HA-FAM134B HeLa TREx cell lysates.

540 (F) Indicated concentrations of polymyxin B (Poly B) were used to inhibit the binding of
541 biotin-conjugated *E. coli* O111:B4 LPS to HA-tagged FAM134B in Dox-induced FLAG-
542 HA-FAM134B HeLa TREx cell lysates.

543 (G) Schematic representation of the full length FAM134B sequence, which is
544 composed of a reticulum homology domain (RHD), N-terminal (Nter, grey) and C-
545 terminal regions (Cter, grey). LC3-interacting region consisting of 4 amino acids (LIR,
546 pink) is located in the C-terminal region. The RHD consists of two transmembrane
547 segments TM12 and TM34 (green), which are connected by a 60-residue linker, and
548 two additional terminal segments. The C-terminal fragment of the RHD (AHC, yellow)
549 and the linker-helix (AHL, yellow) form conserved amphipathic helices. The lower table
550 shows the number of positively charged residues (arginine, R; Lysine, K) and the
551 percentage of solvent accessible in every segment of FAM134B.

552 (H) Substitution of amino acids (R or K to glutamic acid, E) in segment AHL (AHLmt),
553 AHC (AHCmt), and C-terminal (CTERmt). DOUBLEmt 1, DOUBLEmt 2, and
554 TRIPLEmt indicate combination as shown in the table.

555 (I) Streptavidin pulldown assays that determine the binding of the indicated amount of
556 biotin-conjugated *E. coli* O111:B4 LPS to HA-tagged wild type or different mutant
557 FAM134B transfected in HEK293T cells. GAPDH was used as an internal control of
558 input.

559 (J and K) Immunofluorescence staining and quantification of HA and *Salmonella* LPS,
560 and LC3B in FAM134B WT-HA or FAM134B TRIPLEmt-HA transfected HeLa cells
561 infected with SL1344 for 2 hr. Scale bar, 10 μm. (J) Quantification of number of LC3B-
562 positive HA-FAM134B puncta per cell (K). Solid bars of boxes indicate the medians.
563 Boxes represent interquartile range from 25th to 75th percentile, and whiskers indicates
564 10th to 90th percentile. Differences were statistically analyzed by one-way ANOVA and
565 Tukey's multiple comparison test. ***$p < 0.001$. ns, not significant. Data were collected
566 60 cells from three independent biological replicates.

567 (L) Co-IP of LPS and endogenous LC3B-II in FAM134B WT-HA or FAM134B
568 TRIPLEmt-HA transfected HeLa cells, which were infected with SL1344 for 2 hr.
569 GAPDH was used as an internal control of input. The bands at ~ 22kD.

570

571 **Figure 3. O-Ag of LPS induces FAM134B oligomerization and membrane**
572 **fragmentation**

573 (A) Size analysis of S protein-FLAG-Streptavidin binding peptide (SFB)-FAM134B
574 oligomers after incubation with indicated amount of *Salmonella* S-LPS or lipid A by
575 blue native page and immunoblotting of FLAG.

576 (B) Size analysis of SFB-FAM134B oligomers purified from cell lysates infected with
577 NCTC12023 WT or O-Ag mutant (Δ) and complemented (compl.) strains. Upper panel
578 shows lower exposure (Low exp) blot and lower blot shows higher exposure (high exp)
579 blot. GAPDH was used as an internal control of input.

580 (C) Schematic representation of LPS structure of different O-Ag mutant strains,
581 including the strains mutant for *rfbP, rfaL*, *rfaG,* and *rfaH.*

582 (D-E) Representative images (D) and quantitative results (E) of remodeled
583 proteoliposomes (scale bars, 100 nm) taken from negative stain Transmission Electron
584 Microscopy (nsTEM). Empty liposomes (Empty) were added FAM134B-GST
585 recombinant protein at a lipid to protein ratio (LPR) 100:1 without (LPR 100:1) or with
586 0.5 mg/ml LPS (LPR 100:1+LPS 0.5) or 1 mg/ml LPS (LPR 100:1+ LPS 1). Incubation

587 of liposome with 1 mg/ml LPS was taken as negative control to check the effect of LPS
588 on liposome. The diameter of the representative proteoliposome with average size for
589 each group showed by dotted line or arrow.

590 (F-G) Representative images (F) and quantitative results (E) of different LPS, including
591 1 mg/ml of S-LPS, Ra-LPS, and Re-LPS, remodeled proteoliposomes (LPR 100:1,
592 scale bars, 100 nm). The diameter of the representative proteoliposome with average
593 size for each group showed by dotted line or arrow.

594 (E and G) The size distributions (n=300 each) from nsTEM images were measured
595 and showed by violin plots, showing a central boxplot (black lines indicate median with
596 interquartile range) with mirrored histograms on both sides (G).

597 (H and I) Immunofluorescence of HA, *Salmonella* LPS, and LC3B in HeLa TREx
598 inducible cell line expressing FLAG-HA-FAM134B infected with NCTC12023 WT or
599 LPS O-Ag mutant (Δ) and complemented (compl.) strains for 2 hr (H). DAPI staining
600 was used for cell nuclear and bacterial DNA staining. Scale bar, 10 μm. Quantification
601 of LC3B-positive HA-FAM134B puncta per cell (I) and *Salmonella* count per cell (J).
602 Data were collected 60 cells from three independent biological replicates.
603 Representative images are shown in Figure S3C.

604 (E, G, H, I) Differences were statistically analyzed by one-way ANOVA and Tukey's
605 multiple comparison test. *$p<0.05$, **$p<0.01$, ***$p < 0.001$, ns not significant.
606

607 **Figure 4. FAM134B-positive *Salmonella*-containing vacuoles are unacidified,**
608 **promoting *Salmonella* survival**

609 (A-B) Immunofluorescence staining of HA, LC3B, and LAMP1, indicating SCV, in HeLa
610 TREx inducible cell line expressing FLAG-HA-FAM134B infected with SL1344 for 4 hr
611 (A). DAPI was used for cell nuclear and bacterial DNA staining. Scale bar, 10 μm. The
612 percentage of FAM134B and LC3B double-positive *Salmonella* in all LC3B-positive
613 *Salmonella*, as well as the percentage of FAM134B and LAMP1 double-positive
614 *Salmonella* in all LAMP1-positive *Salmonella* was quantified using CellPathfinder
615 software (B). Data presented as mean + sem, n=3, > 400 cells.

616 (C-D) Immunofluorescence staining of HA and LC3B, and lysotracker staining in HeLa
617 TREx inducible cell line expressing FLAG-HA-FAM134B infected with SL1344 for 4 hr
618 (C). DAPI staining was used for cell nuclear and bacterial DNA staining. Scale bar, 10
619 μm. The percentages of lysotracker-positive or negative *Salmonella* to the indicating

620 markers *Salmonella* were quantified (D). Data were collected 60 cells from three
621 independent biological replicates.

622 (E-F) Immunofluorescence staining of LC3B and lysotracker staining in HeLa cells
623 transfected with control siRNA or FAM134B siRNA infected with SL1344 for 4 hr (E).
624 DAPI was used for cell nuclear and bacterial DNA staining. Scale bar, 10 μm. The
625 percentage of lysotracker-positive *Salmonella* to LC3B-positive *Salmonella* (F). Data
626 were collected 60 cells from three independent biological replicates.

627 (G) Colony-forming assay was performed to quantify the bacteria count in HeLa TREx
628 inducible cells expressing FLAG-HA-FAM134B WT or FLAG-HA-FAM134B mtLIR
629 infected with SL1344 for 1 hr and 8 hr. The fold increase of bacteria multiplication was
630 calculated by normalizing bacteria count at 8 hr to 1 hr post-infection.

631 (H-I) Colony-forming assay was performed to quantify the bacteria count in HeLa cell
632 transfected with control siRNA or FAM134B siRNA (H) or FAM134B WT MEF and
633 FAM134B KO MEF infected with SL1344 100 moi at the indicated time points.

634 (B, D, F, G) Data represented as mean + sem. Differences were statistically analyzed
635 by unpaired t-test (F and G) or by two-way ANOVA (H and I). **$p<0.01$, ***$p < 0.001$,
636 ns, not significant.

637

638 **Figure 5. LPS for FAM134B-mediated fragmentation is delivered by OMV**

639 (A-B) Immunofluorescence staining of HA, *Salmonella* LPS, and LC3B in cells infected
640 with different mutant strains, including Δ*ompA*, Δ*tolAB*, and Δ*degS*, and Δ*pagL* strains.
641 DAPI was used for cell nuclear and bacterial DNA staining. Scale bar, 10 μm.
642 Quantification of LC3B-positive HA-FAM134B puncta (A) and *Salmonella* count per
643 cell (B). Representative images are shown in Figure S7D.

644 (C) Co-IP of LPS with HA in cells infected with NCTC12023 WT or indicated mutant
645 strains for 2 hr. GAPDH was used as an internal control of input.

646 (D-E) Immunofluorescence staining of HA, *Salmonella* LPS, and LC3B in cells treated
647 with purified SL1344 OMVs for 6 hr (D). DAPI was used for cell nuclear DNA staining.
648 Scale bar, 10 μm. Quantification of LC3B-positive HA-FAM134B puncta cell per cell
649 (E).

650 (F) Immunofluorescence staining of HA and LC3B in cells treated with purified OMVs
651 form NCTC12023 WT or indicated mutant strains for 6 hr. DAPI was used for cell
652 nuclear DNA staining. Scale bar, 10 μm. Quantification of LC3B-positive HA-FAM134B
653 puncta per cell (F).

654 (G-H) Immunofluorescence staining of HA and LC3B in cells infected by EPEC or BL21
655 directly or with 0.45 μm transwell for 4 hr (G). DAPI was used for cell nuclear DNA
656 staining. Scale bar, 10 μm. Quantification of LC3B-positive HA-FAM134B puncta cell
657 per cell (H).

658 (I) Immunofluorescence staining of HA and LC3B in cells treated with purified OMVs
659 form EPEC or BL21 for 6 hr. Quantification of LC3B-positive HA-FAM134B puncta cell
660 per cell with OMVs, stained by DiO Vybrant. Representative images are shown in
661 Figure S8B.

662 HeLa TREx inducible cell lines expressing FLAG-HA-FAM134B was used for all
663 experiments in Fig. 5. (A, B, E, F, H, and I) Solid bars of boxes indicate the medians.
664 Boxes represent interquartile range from 25th to 75th percentile, and whiskers indicates
665 10th to 90th percentile. Differences were statistically analyzed by one-way ANOVA and
666 Tukey's multiple comparison test. ***$p < 0.001$, ns, not significant. Data were collected
667 60 cells from two (A, B and H) three independent (E, F and I) biological replicates.
668
669 **STAR METHODS**
670 LEAD CONTACT AND MATERIALS AVAILABILITY
671 Further information and requests for reagents may be directed to and will be fulfilled
672 by the Lead Contact Ivan Dikic (ivan.dikic@biochem2.de). All unique/ stable reagents
673 generated in this study are available from the LEAD Contact with a completed materials
674 transfer agreement (MTA).
675
676 EXPERIMENTAL MODEL AND SUBJECT DETAILS
677
678 Mammalian cell culture
679
680 HeLa and HEK293T cells were obtained from American Type Culture Collection
681 (ATCC). WT and Fam 134b KO MEFs and BMDMs were isolated from respective mice
682 genotypes. Animal experiments are approved by the Thüringer Landesamt für
683 Lebensmittelsicherheit und Verbraucherschutz (TLV) (license number UKJ 22-019).
684 MEFs were isolated and cultured from E13.5 stage embryos and SV40 large T antigen
685 plasmid was used to immortalize MEFs. To culture BMDMs, femur and tibia bones

686 were isolated from 12-16 week old WT and Fam134b KO mice after euthanasia. The
687 bones were cleaned, sterilized, and the bone marrow was flushed out with sterile PBS.
688 It was centrifuged and re-suspended with BMDM culture media (DMEM supplemented
689 with 10% fetal bovine serum, 1% penicillin/streptomycin and 20 ng/mL of murine
690 macrophage colony-stimulating factor), and plated in petri dishes. Fresh media was
691 added on day 2. By day 5, differentiated macrophages were attached and the debris
692 were removed, the cells were washed with 1x PBS, collected, counted, and plated for
693 the experiments. Flp-In HeLa TREx cell lines (Invitrogen) were used to generate
694 inducible cell lines by cloning the cDNAs of FAM134B, FAM134B mtLIR (DDFELLD
695 LIR substituted by seven alanine residues), and RTN3L into MSCV iTAP N-FLAG-HA
696 retroviral vector. Then, 2 µg/ml puromycin and 15 µg/ml blasticidin were treated for
697 selection and maintenance of stable cells. Cells were cultured in Dulbecco's Modified
698 Eagle's Medium (DMEM) supplemented with 10% fetal bovine serum, 1%
699 penicillin/streptomycin at 37°C with 5% CO2. BMDMs were additionally supplemented
700 with 20 ng/mL of murine macrophage colony-stimulating factor (Miltenyi BioTech).
701
702 Microbe strains
703
704 *S.* Typhimurium strains used in this study. The following isogenic mutant and
705 complemented NCTC12023 strains were established by Prof. Dr. Michael Hensel
706 (Zenk *et al.*, 2009).
707
708 1. SL1344 (WT)
709 2. NCTC12023 (WT)
710 3. NCTC12023 strains with deletion on *ompA, tolAB, degS* or *pagL.*
711 Mutant strains of *S. enterica* serovar Typhimurium strain NCTC12023 were
712 generated by λ Red-mediated homologous recombination basically as described
713 before (Datsenko and Wanner, 2000), using pWRG730 as helper plasmid for
714 controlled expression of Red functions (Hoffmann et al., 2017). The 60-mer
715 oligonucleotide sets as listed in Table X were used to amplify the *aph* targeting
716 cassette using pKD13 (for *tolA*, *degS*, or *ompA*) or pKD4 (for *pagL*) as template DNA.
717 Proper insertion of *aph* cassettes into target genes was confirmed by colony PCR
718 using gene-specific check primers flanking deletions, and universal K1 Red Del.
719 Confirmed mutated alleles were moved into fresh strain background using P22
720 transduction. The effects of mutations on outer membrane integrity were analysed
721 by SEM and nsTEM of strains grown overnight on LB agar (Fig. S7)
722 4. NCTC12023 strains with deletion on *rfbP, rfaL, rfaG,* or *rfaH*.
723 Mutant of *rfbP* (O-Ag transferase; NP_461027; Δ*rfbP*) and *rfaL* (O-Ag ligase;

724 NP_462613; Δ*rfaL*) are defective in the addition of the O-Ag to the outer core. Mutant
725 of *rfaG* (glucosyltransferase I; NP_462622; Δ*rfaG*) caused outer core cannot be
726 added to inner core. Mutant of *rfaH* (transcriptional activator; NP_ 462862; Δ*rfaH*),
727 which is the gene regulates the stability of the long mRNA for LPS biosynthesis
728 genes, also reduced polymeric O-Ag.
729 5. NCTC12023 strains with complementation of deletion of *rfaL* and *rfaG*
730
731 *E. coli* strains used in this study.
732 1. NEB Turbo
733 2. EPEC O127:H6 (A kind gift from Prof. Dr. Volkhard A. J. Kempf)
734 3. BL21
735 Chemically competent NEB Turbo cells were used for plasmid amplification.
736
737 METHOD DETAILS
738
739 Bacterial infection
740
741 *S.* Typhimurium and *E. coli* were cultured overnight and then diluted at ratio of 1
742 to 33 in fresh LB broth. The diluted cultures were then grown at 37°C for 3 h. For
743 infection, the resuspended bacteria were adjusted to OD600 of 1 and added to HeLa
744 cells or MEFs at a MOI of 100, and BMDMs at a MOI of 10 without antibiotics. After 30
745 min of infection, media were replaced by medium with 100 μg/ml gentamicin to remove
746 extracellular bacteria. Samples were collected at the indicated time points after
747 infection. For colony forming assay, which was performed as previously described
748 (Steele-Mortimer, 2008), after 10 min of *S.* Typhimurium infection, the cells were
749 washed by PBS twice to removed extracellular bacteria and incubated in antibiotics-
750 free DMEM for 20 min. Then, the media were changed to DMEM containing 50 μg/ml
751 gentamicin for 40 min and replaced by DMEM containing 5 μg/ml gentamicin. The cells
752 were lysed with lysis buffer (1% Triton X-100 and 0.1% SDS in PBS) at indicated time
753 points and serial diluted by PBS and plated onto LB plates. After 24 h incubation at
754 37°C, the colonies were calculated.
755
756 Immunofluorescence staining and confocal imaging
757
758 Cells which seeded in the 6-well plates with cover slips fixed by 4%
759 paraformaldehyde in PBS for 15 min at room temperature. The buffer with 0.1%
760 saponin, 1% bovine serum albumin (BSA), 0.05% NaN3 in PBS was used for
761 permeabilization and blocking for 1 h at room temperature. Samples were then probed

762 by indicated primary antibodies as well as Alexa 488, Alexa 546, and Alexa 633
763 fluorescently labelled secondary antibodies (Invitrogen). After DAPI staining for
764 nucleus and bacteria DNA, the samples were fixed by mounting medium. Confocal
765 imaging was done using a Zeiss LSM 780 confocal microscope and analyzed by Zeiss
766 Zen (black edition) software. For high-throughput confocal imaging, cells were seeded
767 in the 96-well black plates with glass bottom followed by immunofluorescence staining
768 and imaging by CellVoyager CQ1 (Yokogawa) system and quantified using
769 CellPathfinder software.
770
771 Immunoprecipitation and western blotting
772
773 For immunoprecipitation, cells were lysed by the lysis buffer containing 50 mM
774 Tris-HCl (pH 7.5),150 mM NaCl, 5 mM EDTA, and 1% NP-40 with protease inhibitor
775 cocktail (Sigma Aldrich). Lysates were incubated with 15 μl anti-HA agarose beads
776 (SantaCruz Biotechnology) overnight at 4°C with end-to-end rotation. Beads were
777 washed three times with wash buffer containing 50 mM Tris-HCl (pH 7.5), 400 mM
778 NaCl, 5 mM EDTA). Proteins were eluted with 2X loading dye by boiling for 10 min
779 followed by western blotting. For western blotting, cells were lysed by the lysis buffer
780 containing 50 mM Tris-HCl (pH 7.5), 150 mM NaCl, 5 mM EDTA, and 1% Triton X-100
781 with protease inhibitor cocktail (Sigma Aldrich). After protein quantification, samples
782 were boiled with loading dyes for 10 min. Samples were separated by running SDS-
783 PAGE with Tris-Glycine gels followed by transferred to PVDF membranes, which were
784 then blocked with 5% milk in TBST. After blocking, the membranes were sequentially
785 hybridized with primary and HRP (horseradish peroxidase) conjugated secondary
786 antibodies. the chemiluminescence method was performed to detect proteins
787 expression.
788
789 Transfection of siRNA
790 Cells were seeded in the 6-well plates on a day before experiments. FAM134B
791 siRNA and Scramble siRNA (Eurofins) were transfection by lipofectamine RNAiMAX
792 (Invitrogen) as manufacturer's instruction. After 48 hr culture, cells were reseeded for
793 the following experiments.
794
795 Streptavidin pulldown assay
796
797 To immobilize LPS onto streptavidin agarose beads, the indicated amount of
798 biotin-conjugated *E. coli* O111:B4 LPS (InvivoGen) were added to 10 μl of streptavidin
799 agarose beads and incubated at 4°C with rotation for 1 hr. The beads were then

800 washed 3 times with the lysis buffer containing 50 mM Tris-HCl (pH 7.5), 150 mM NaCl,
801 5 mM EDTA, and 1% NP-40 to remove unconjugated ligands. Inducible TREx HeLa
802 cells of FLAG-HA-FAM134B and FLAG-HA-RTN3 induced by treatment of 1 μg/ml
803 doxycycline for 24 hr or HEK cells transfected with indicated plasmids were lysed and
804 collected in the lysis buffer supplemented with a protease inhibitor mixture. Cell lysates
805 were precleared by incubating with streptavidin Sepharose at 4°C with rotation for 1 hr.
806 Supernatants were transferred to a new microtube and incubated with biotin-LPS-
807 immobilized streptavidin agarose beads overnight at 4°C with rotation. The beads were
808 then washed three times with wash buffer containing 50 mM Tris-HCl (pH 7.5), 400
809 mM NaCl, 5 mM EDTA and eluted in 2X loading dye by boiling for 10 min followed by
810 western blotting to detect the binding proteins. For competition assay, 50 μg of
811 unlabeled S-LPS, Ra-LPS, Re-LPS, lipid A, and MDP were first incubated with pre-
812 cleared lysates at 4°C for 1 hr with rotation before adding biotinylated LPS-immobilized
813 streptavidin beads. For examination of polymyxin B effect, the indicated concentrations
814 of polymyxin B were first added to biotinylated LPS-immobilized streptavidin beads and
815 incubate with rotation for 0.5 hr. After twice washes by lysis buffer, the pre-cleared
816 lysates were added.
817
818 FAM134B protein purification
819
820 For purification of FAM134B protein from HEK293T cells, the plasmid of S protein-
821 FLAG-Streptavidin binding peptide (SFB)-FAM134B was transfected to HEK293T cells.
822 Cells were lysed with the lysis buffer containing 50 mM Tris-HCl, pH 7.4,150 mM NaCl,
823 0.5 mM EDTA, and 1% TritonX-100. After centrifuge at 17,000 g, 15 min, the lysates
824 were collected and incubated with streptavidin Sepharose (Cytiva) at constant agitation
825 at 4 °C, overnight. After washing three time with the buffers (50 mM Tris, pH=7.4,150
826 mM NaCl, 0.5 mM EDTA) containing 0.5 % NP-40, 0.3 % NP-40 and 0.1 % NP-40,
827 respectively, the buffers were removed and the SFB-FAM134B protein on the
828 Sepharose was further eluted by incubated with 2 mM D-biotin dissolved in the buffer
829 containing 50 mM Tris-HCl, pH 7.4,150 mM NaCl, 0.5 mM EDTA, and 0.1% NP-40 for
830 1 hr at 4°C with constant agitation at 800 rpm. The eluted SFB-FAM134B was collected
831 for blue native page analysis.
832 Recombinant GST-FAM134B was purified from *E. coli* for Liposome-remodeling
833 assay as previous described (Gonzalez *et al.*, 2023). Briefly, Fam134B-GST plasmids
834 were transformed into BL21DE3 strain of *E. coli*, and a single colony was used to grow
835 the primary culture in the presence of appropriate antibiotic (ampicillin). The overnight
836 grown primary cultures were used to inoculate secondary cultures and allowed to grow
837 up to a OD of 0.6 by shaking at 200 rpm and 37 °C, followed by induction of the cultures

838 using 0.5 mM of IPTG for 3 hours. The cells were harvested, suspended in ice cold
839 PBS and lysed using sonication, centrifuged (10,000 xg) to separate the supernatant
840 and pellet. The resultant supernatant was further fractioned by ultracentrifugation at
841 80,000g for 100 minutes at 4 °C. The pellet fractions were dissolved in PBS buffer
842 containing dodecyl β-D-maltoside (DDM; 0.05%), followed by affinity purification using
843 glutathione-Sepharose TM4 Fast Flow columns (GE Healthcare). The protein was
844 eluted from the column using PBS containing 10 mM reduced glutathione and 0.05%
845 DDM. The fractions containing Fam134B-GST protein were concentrated and buffered
846 exchanged with storage buffer (50 mM HEPES pH 7.5, 150 mM NaCl) containing
847 0.0075%DDM.
848
849 Blue native page

850 Blue native page analysis was performed as previous described with slight
851 modifications (Jiang *et al.*, 2020; Wittig *et al.*, 2006). SFB-FAM134B protein was
852 incubated with indicated amount of S-LPS or lipid A at 37°C for 2 hr. Then, the mixture
853 was incubated with 2 μl 50% glycerol and 3 μl 0.1% Coomassie blue G-250 for 15 min
854 at room temperature followed by loading to 4%–12% gradient native PAGE gel (Bio-
855 Rad), running in blue cathode/anode buffer (Invitrogen) for 2 hr at 150 V in an ice bath.
856 The gels were further transfer to PVDF membranes by electroblotting followed by
857 detection with anti-FLAG antibody.

858 Liposome preparation

859 Liposomes were prepared as previous described (Bhaskara *et al.*, 2019). In brief,
860 two kinds of lipids,1,2-dioleoyl-sn-glycero-3-phosphocholine (DOPC, Avanti Polar
861 Lipids Inc.) and 1,2-dioleoyl-sn-glycero-3-phosphoethanolamine (DOPE, Avanti Polar
862 Lipids Inc.), were dissolved in a mixture of chloroform and methanol (4:1) in a glass
863 flask to obtain the molar ratio of 0.8:0.2 (DOPC:DOPE). The organic solvent was then
864 evaporated to get a dry lipid film, which was then hydrated with liposome buffer (50
865 mM HEPES, 150 mM NaCl buffer at pH 7.4) to a final concentration 15 mg/ml lipid
866 solution. The liposomes were formed by sonication in an ultrasound bath followed by
867 flash-freeze in liquid nitrogen and slowly thaw in room temperature for 10 times cycles.
868 The hydrated liposomes were further extruded by a lipid extruder (Avanti Polar Lipids
869 Inc.) with 200 nm polycarbonate membranes (Avanti Polar Lipids) for 21 times.

870 Liposome-remodeling assay

871 Liposome-remodeling assay was performed as previous described with minor
872 modifications (Bhaskara *et al.*, 2019). Liposomes and the purified FAM134B-GST

873 protein were mixed at an indicated lipid-to-protein ratio (LPR) and incubated for 18 h
874 at 22 °C in 30 μL of liposome buffer with constant agitation (600 rpm). To investigate
875 the effect of different LPS, FAM134B-GST protein was first added to liposome at LPR
876 100:1 for 1 h, then added LPS to the proteoliposome and incubated for 17 h at 22 °C.
877 All the samples were assessed by negative-stain transmission electron microscopy.
878 For imaging, samples were first diluted to a final lipid concentration of 1 mg/ml by
879 liposome buffer. 5 μl of each diluted sample was deposited to the carbon-coated
880 copper grids (SPI Supplies), which were already glow-discharged for 20 s at 15 mA
881 and 0.38 mbar vacuum. After 1 minute incubation and washes with buffer for twice, 1%
882 uranyl formate was subsequently used to stain the grids for 10 seconds at room
883 temperature. A 120 kV Tecnai Spirit Biotwin electron microscope (FEI) equipped with
884 a 4k × 4k CCD detector (US4000-1, Gatan) was used to taken 10 micrographs for each
885 sample. Image J software was used to measure the sizes (diameters) of 300
886 proteoliposomes for each sample.

887 OMV isolation

888 0.5 L overnight grown bacterial cultures were harvested for OMV isolation. Bacterial
889 cells were first removed by centrifugation (12,000 g for 15 min), the supernatant was
890 filtered through 0.45 μm PVDF membrane, the filtered broth concentrated to 50 ml
891 (Vivaflow 200, 100,000 MWCO PES, Sartorius), and the OMVs were pelleted by
892 ultracentrifugation at 60,000 rpm (369548.3 g) for 1 hr at 4 °C. The OMVs were washed
893 with PBS and pelleted again by ultracentrifugation. The OMVs were resuspended in
894 0.5 ml PBS. In the cases which needed to do immunofluorescence labeling, Vybrant
895 DiO cell labeling dye (ThermoFisher Scientific) was added at 1:50 and incubated at
896 37 °C for 20 min. After labeling, the excess dye was removed and washed by PBS
897 three times at 3000 rpm (956 g) by Micron 10 kDa centrifugal filter units (Millipore) in a
898 benchtop centrifuge. The OMVs were further sterilized by syringe filters (0.22 um) and
899 measured concentration by bicinchoninic acid assay (BCA) method. OMVs were
900 added to the cells at concentration of 25 μg/ml.

901 Quantification and statistical analysis

902 GraphPad Prism 8 was used to do statistical analysis. Comparisons of two variables
903 were analyzed by unpaired and two-tailed Student's t tests. For three or more sets of
904 data, statistics were performed by one-way ANOVA with Tukey's multiple comparison
905 post test. * indicates $p < 0.05$, ** indicates $p < 0.01$, *** indicates $p < 0.001$. N
906 represents the number of independent biological replicates. Data are represented as
907 mean ± sem.

908

909 **REFERENCES**

910

911 Adams, P.G., Lamoureux, L., Swingle, K.L., Mukundan, H., and Montano, G.A.
912 (2014). Lipopolysaccharide-induced dynamic lipid membrane reorganization:
913 tubules, perforations, and stacks. Biophys J *106*, 2395-2407.
914 10.1016/j.bpj.2014.04.016.
915 Aglietti, R.A., Estevez, A., Gupta, A., Ramirez, M.G., Liu, P.S., Kayagaki, N., Ciferri,
916 C., Dixit, V.M., and Dueber, E.C. (2016). GsdmD p30 elicited by caspase-11
917 during pyroptosis forms pores in membranes. Proc Natl Acad Sci U S A *113*,
918 7858-7863. 10.1073/pnas.1607769113.
919 An, H., Ordureau, A., Paulo, J.A., Shoemaker, C.J., Denic, V., and Harper, J.W.
920 (2019). TEX264 Is an endoplasmic reticulum-resident ATG8-interacting protein
921 critical for ER remodeling during nutrient stress. Mol Cell *74*, 891-908 e810.
922 10.1016/j.molcel.2019.03.034.
923 Bakowski, M.A., Braun, V., Lam, G.Y., Yeung, T., Heo, W.D., Meyer, T., Finlay, B.B.,
924 Grinstein, S., and Brumell, J.H. (2010). The phosphoinositide phosphatase
925 SopB manipulates membrane surface charge and trafficking of the
926 Salmonella-containing vacuole. Cell Host Microbe *7*, 453-462.
927 10.1016/j.chom.2010.05.011.
928 Bhaskara, R.M., Grumati, P., Garcia-Pardo, J., Kalayil, S., Covarrubias-Pinto, A.,
929 Chen, W., Kudryashev, M., Dikic, I., and Hummer, G. (2019). Curvature
930 induction and membrane remodeling by FAM134B reticulon homology domain
931 assist selective ER-phagy. Nat Commun *10*, 2370. 10.1038/s41467-019-
932 10345-3.
933 Chen, Q., Xiao, Y., Chai, P., Zheng, P., Teng, J., and Chen, J. (2019). ATL3 Is a
934 tubular ER-phagy receptor for GABARAP-mediated selective autophagy. Curr
935 Biol *29*, 846-855 e846. 10.1016/j.cub.2019.01.041.
936 Chino, H., Hatta, T., Natsume, T., and Mizushima, N. (2019). Intrinsically disordered
937 protein TEX264 mediates ER-phagy. Mol Cell *74*, 909-921 e906.
938 10.1016/j.molcel.2019.03.033.
939 Chino, H., and Mizushima, N. (2020). ER-phagy: quality control and turnover of
940 endoplasmic reticulum. Trends Cell Biol *30*, 384-398.
941 10.1016/j.tcb.2020.02.001.
942 Datsenko, K.A., and Wanner, B.L. (2000). One-step inactivation of chromosomal
943 genes in Escherichia coli K-12 using PCR products. Proc Natl Acad Sci U S A
944 *97*, 6640-6645. 10.1073/pnas.120163297.
945 Deatherage, B.L., Lara, J.C., Bergsbaken, T., Rassoulian Barrett, S.L., Lara, S., and

946 Cookson, B.T. (2009). Biogenesis of bacterial membrane vesicles. Mol
947 Microbiol *72*, 1395-1407. 10.1111/j.1365-2958.2009.06731.x.
948 Ding, J., Wang, K., Liu, W., She, Y., Sun, Q., Shi, J., Sun, H., Wang, D.C., and Shao,
949 F. (2016). Pore-forming activity and structural autoinhibition of the gasdermin
950 family. Nature *535*, 111-116. 10.1038/nature18590.
951 Elhenawy, W., Bording-Jorgensen, M., Valguarnera, E., Haurat, M.F., Wine, E., and
952 Feldman, M.F. (2016). LPS Remodeling Triggers Formation of Outer
953 Membrane Vesicles in Salmonella. mBio *7*. 10.1128/mBio.00940-16.
954 Escoll, P., Mondino, S., Rolando, M., and Buchrieser, C. (2016). Targeting of host
955 organelles by pathogenic bacteria: a sophisticated subversion strategy. Nat
956 Rev Microbiol *14*, 5-19. 10.1038/nrmicro.2015.1.
957 Fumagalli, F., Noack, J., Bergmann, T.J., Cebollero, E., Pisoni, G.B., Fasana, E.,
958 Fregno, I., Galli, C., Loi, M., Solda, T., et al. (2016). Translocon component
959 Sec62 acts in endoplasmic reticulum turnover during stress recovery. Nat Cell
960 Biol *18*, 1173-1184. 10.1038/ncb3423.
961 Garcia-del Portillo, F., Stein, M.A., and Finlay, B.B. (1997). Release of
962 lipopolysaccharide from intracellular compartments containing Salmonella
963 typhimurium to vesicles of the host epithelial cell. Infect Immun *65*, 24-34.
964 10.1128/iai.65.1.24-34.1997.
965 Gatica, D., Alsaadi, R.M., Hamra, R.E., Mueller, R., Miyazaki, M., Sad, S., and
966 Russell, R.C. (2024). The ER-phagy receptor FAM134B is targeted by
967 *Salmonella* Typhimurium to promote infection. bioRxiv,
968 2024.2003.2028.587227. 10.1101/2024.03.28.587227.
969 Gonzalez, A., Covarrubias-Pinto, A., Bhaskara, R.M., Glogger, M., Kuncha, S.K.,
970 Xavier, A., Seemann, E., Misra, M., Hoffmann, M.E., Brauning, B., et al.
971 (2023). Ubiquitination regulates ER-phagy and remodelling of endoplasmic
972 reticulum. Nature. 10.1038/s41586-023-06089-2.
973 Grumati, P., Morozzi, G., Holper, S., Mari, M., Harwardt, M.I., Yan, R., Muller, S.,
974 Reggiori, F., Heilemann, M., and Dikic, I. (2017). Full length RTN3 regulates
975 turnover of tubular endoplasmic reticulum via selective autophagy. Elife *6*.
976 10.7554/eLife.25555.
977 Gubas, A., and Dikic, I. (2022). ER remodeling via ER-phagy. Mol Cell *82*, 1492-
978 1500. 10.1016/j.molcel.2022.02.018.
979 Hoffmann, S., Schmidt, C., Walter, S., Bender, J.K., and Gerlach, R.G. (2017).
980 Scarless deletion of up to seven methyl-accepting chemotaxis genes with an
981 optimized method highlights key function of CheM in Salmonella Typhimurium.
982 PLoS One *12*, e0172630. 10.1371/journal.pone.0172630.
983 Jiang, X., Wang, X., Ding, X., Du, M., Li, B., Weng, X., Zhang, J., Li, L., Tian, R., Zhu,

984 Q., et al. (2020). FAM134B oligomerization drives endoplasmic reticulum
985 membrane scission for ER-phagy. EMBO J *39*, e102608.
986 10.15252/embj.2019102608.
987 Juodeikis, R., and Carding, S.R. (2022). Outer membrane vesicles: biogenesis,
988 functions, and issues. Microbiol Mol Biol Rev *86*, e0003222.
989 10.1128/mmbr.00032-22.
990 Kawasaki, K., Ernst, R.K., and Miller, S.I. (2004). 3-O-deacylation of lipid A by PagL,
991 a PhoP/PhoQ-regulated deacylase of Salmonella typhimurium, modulates
992 signaling through Toll-like receptor 4. J Biol Chem *279*, 20044-20048.
993 10.1074/jbc.M401275200.
994 Khaminets, A., Heinrich, T., Mari, M., Grumati, P., Huebner, A.K., Akutsu, M.,
995 Liebmann, L., Stolz, A., Nietzsche, S., Koch, N., et al. (2015). Regulation of
996 endoplasmic reticulum turnover by selective autophagy. Nature *522*, 354-358.
997 10.1038/nature14498.
998 Kumar, D., Lak, B., Suntio, T., Vihinen, H., Belevich, I., Viita, T., Xiaonan, L.,
999 Vartiainen, A., Vartiainen, M., Varjosalo, M., and Jokitalo, E. (2021). RTN4B
1000 interacting protein FAM134C promotes ER membrane curvature and has a
1001 functional role in autophagy. Mol Biol Cell *32*, 1158-1170. 10.1091/mbc.E20-
1002 06-0409.
1003 Kutsch, M., Sistemich, L., Lesser, C.F., Goldberg, M.B., Herrmann, C., and Coers, J.
1004 (2020). Direct binding of polymeric GBP1 to LPS disrupts bacterial cell
1005 envelope functions. EMBO J *39*, e104926. 10.15252/embj.2020104926.
1006 LaRock, D.L., Chaudhary, A., and Miller, S.I. (2015). Salmonellae interactions with
1007 host processes. Nat Rev Microbiol *13*, 191-205. 10.1038/nrmicro3420.
1008 Madan, R., Rastogi, R., Parashuraman, S., and Mukhopadhyay, A. (2012).
1009 Salmonella acquires lysosome-associated membrane protein 1 (LAMP1) on
1010 phagosomes from Golgi via SipC protein-mediated recruitment of host
1011 Syntaxin6. J Biol Chem *287*, 5574-5587. 10.1074/jbc.M111.286120.
1012 Man, S.M., Karki, R., Sasai, M., Place, D.E., Kesavardhana, S., Temirov, J., Frase,
1013 S., Zhu, Q., Malireddi, R.K.S., Kuriakose, T., et al. (2016). IRGB10 liberates
1014 bacterial ligands for sensing by the AIM2 and caspase-11-NLRP3
1015 inflammasomes. Cell *167*, 382-396 e317. 10.1016/j.cell.2016.09.012.
1016 Meunier, E., Dick, M.S., Dreier, R.F., Schurmann, N., Kenzelmann Broz, D., Warming,
1017 S., Roose-Girma, M., Bumann, D., Kayagaki, N., Takeda, K., et al. (2014).
1018 Caspase-11 activation requires lysis of pathogen-containing vacuoles by IFN-
1019 induced GTPases. Nature *509*, 366-370. 10.1038/nature13157.
1020 Moretti, J., Roy, S., Bozec, D., Martinez, J., Chapman, J.R., Ueberheide, B.,
1021 Lamming, D.W., Chen, Z.J., Horng, T., Yeretssian, G., et al. (2017). STING

1022 senses microbial viability to orchestrate stress-mediated autophagy of the
1023 endoplasmic reticulum. Cell *171*, 809-823 e813. 10.1016/j.cell.2017.09.034.
1024 Nevermann, J., Silva, A., Otero, C., Oyarzun, D.P., Barrera, B., Gil, F., Calderon, I.L.,
1025 and Fuentes, J.A. (2019). Identification of genes involved in biogenesis of
1026 outer membrane vesicles (OMVs) in *Salmonella enterica* Serovar Typhi. Front
1027 Microbiol *10*, 104. 10.3389/fmicb.2019.00104.
1028 Nthiga, T.M., Kumar Shrestha, B., Sjottem, E., Bruun, J.A., Bowitz Larsen, K.,
1029 Bhujabal, Z., Lamark, T., and Johansen, T. (2020). CALCOCO1 acts with
1030 VAMP-associated proteins to mediate ER-phagy. EMBO J *39*, e103649.
1031 10.15252/embj.2019103649.
1032 Park, B.S., Song, D.H., Kim, H.M., Choi, B.S., Lee, H., and Lee, J.O. (2009). The
1033 structural basis of lipopolysaccharide recognition by the TLR4-MD-2 complex.
1034 Nature *458*, 1191-1195. 10.1038/nature07830.
1035 Perrin, A.J., Jiang, X., Birmingham, C.L., So, N.S., and Brumell, J.H. (2004).
1036 Recognition of bacteria in the cytosol of Mammalian cells by the ubiquitin
1037 system. Curr Biol *14*, 806-811. 10.1016/j.cub.2004.04.033.
1038 Ravenhill, B.J., Boyle, K.B., von Muhlinen, N., Ellison, C.J., Masson, G.R., Otten,
1039 E.G., Foeglein, A., Williams, R., and Randow, F. (2019). The Cargo Receptor
1040 NDP52 Initiates Selective Autophagy by Recruiting the ULK Complex to
1041 Cytosol-Invading Bacteria. Mol Cell *74*, 320-329 e326.
1042 10.1016/j.molcel.2019.01.041.
1043 Reggio, A., Buonomo, V., Berkane, R., Bhaskara, R.M., Tellechea, M., Peluso, I.,
1044 Polishchuk, E., Di Lorenzo, G., Cirillo, C., Esposito, M., et al. (2021). Role of
1045 FAM134 paralogues in endoplasmic reticulum remodeling, ER-phagy, and
1046 Collagen quality control. EMBO Rep *22*, e52289. 10.15252/embr.202052289.
1047 Santos, J.C., Boucher, D., Schneider, L.K., Demarco, B., Dilucca, M., Shkarina, K.,
1048 Heilig, R., Chen, K.W., Lim, R.Y.H., and Broz, P. (2020). Human GBP1 binds
1049 LPS to initiate assembly of a caspase-4 activating platform on cytosolic
1050 bacteria. Nat Commun *11*, 3276. 10.1038/s41467-020-16889-z.
1051 Santos, N.C., Silva, A.C., Castanho, M.A., Martins-Silva, J., and Saldanha, C. (2003).
1052 Evaluation of lipopolysaccharide aggregation by light scattering spectroscopy.
1053 Chembiochem *4*, 96-100. 10.1002/cbic.200390020.
1054 Schwechheimer, C., and Kuehn, M.J. (2015). Outer-membrane vesicles from Gram-
1055 negative bacteria: biogenesis and functions. Nat Rev Microbiol *13*, 605-619.
1056 10.1038/nrmicro3525.
1057 Shi, J., Zhao, Y., Wang, Y., Gao, W., Ding, J., Li, P., Hu, L., and Shao, F. (2014).
1058 Inflammatory caspases are innate immune receptors for intracellular LPS.
1059 Nature *514*, 187-192. 10.1038/nature13683.

1060 Siggel, M., Bhaskara, R.M., Moesser, M.K., I, D.I., and Hummer, G. (2021).
1061 FAM134B-RHD protein clustering drives spontaneous budding of asymmetric
1062 membranes. J Phys Chem Lett *12*, 1926-1931. 10.1021/acs.jpclett.1c00031.
1063 Silhavy, T.J., Kahne, D., and Walker, S. (2010). The bacterial cell envelope. Cold
1064 Spring Harb Perspect Biol *2*, a000414. 10.1101/cshperspect.a000414.
1065 Smith, M.D., Harley, M.E., Kemp, A.J., Wills, J., Lee, M., Arends, M., von Kriegsheim,
1066 A., Behrends, C., and Wilkinson, S. (2018). CCPG1 Is a non-canonical
1067 autophagy cargo receptor essential for ER-phagy and pancreatic ER
1068 proteostasis. Dev Cell *44*, 217-232 e211. 10.1016/j.devcel.2017.11.024.
1069 Steele-Mortimer, O. (2008). Infection of epithelial cells with Salmonella enterica.
1070 Methods Mol Biol *431*, 201-211. 10.1007/978-1-60327-032-8_16.
1071 Szczepaniak, J., Press, C., and Kleanthous, C. (2020). The multifarious roles of Tol-
1072 Pal in Gram-negative bacteria. FEMS Microbiol Rev *44*, 490-506.
1073 10.1093/femsre/fuaa018.
1074 Vanaja, S.K., Russo, A.J., Behl, B., Banerjee, I., Yankova, M., Deshmukh, S.D., and
1075 Rathinam, V.A.K. (2016). Bacterial outer membrane vesicles mediate cytosolic
1076 localization of LPS and caspase-11 activation. Cell *165*, 1106-1119.
1077 10.1016/j.cell.2016.04.015.
1078 Wild, P., Farhan, H., McEwan, D.G., Wagner, S., Rogov, V.V., Brady, N.R., Richter, B.,
1079 Korac, J., Waidmann, O., Choudhary, C., et al. (2011). Phosphorylation of the
1080 autophagy receptor optineurin restricts Salmonella growth. Science *333*, 228-
1081 233. 10.1126/science.1205405.
1082 Wittig, I., Braun, H.P., and Schagger, H. (2006). Blue native PAGE. Nat Protoc *1*,
1083 418-428. 10.1038/nprot.2006.62.
1084 Zenk, S.F., Jantsch, J., and Hensel, M. (2009). Role of Salmonella enterica
1085 lipopolysaccharide in activation of dendritic cell functions and bacterial
1086 containment. J Immunol *183*, 2697-2707. 10.4049/jimmunol.0900937.
1087

Figure 1 Cheng et al

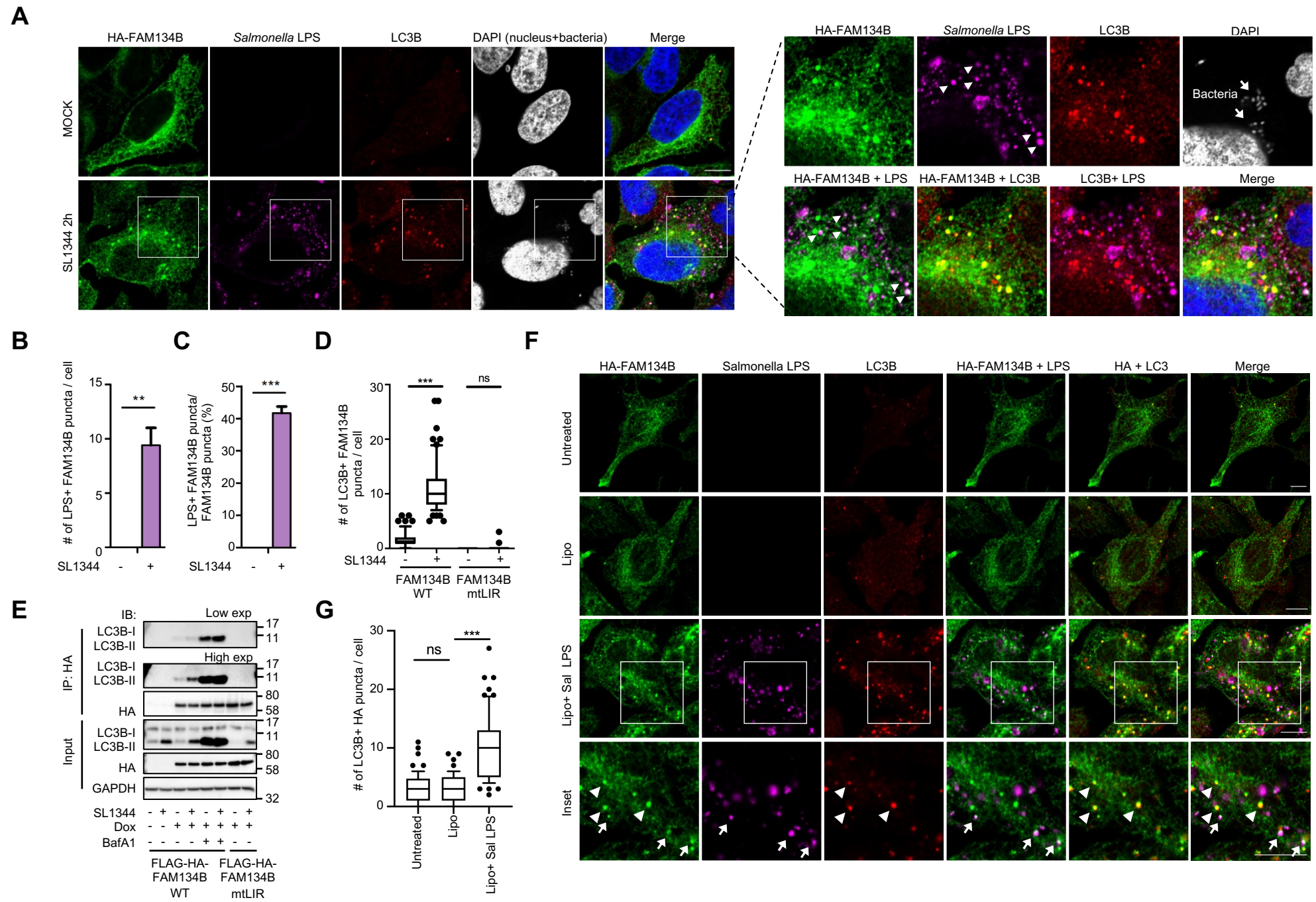

Figure 2 Cheng et al

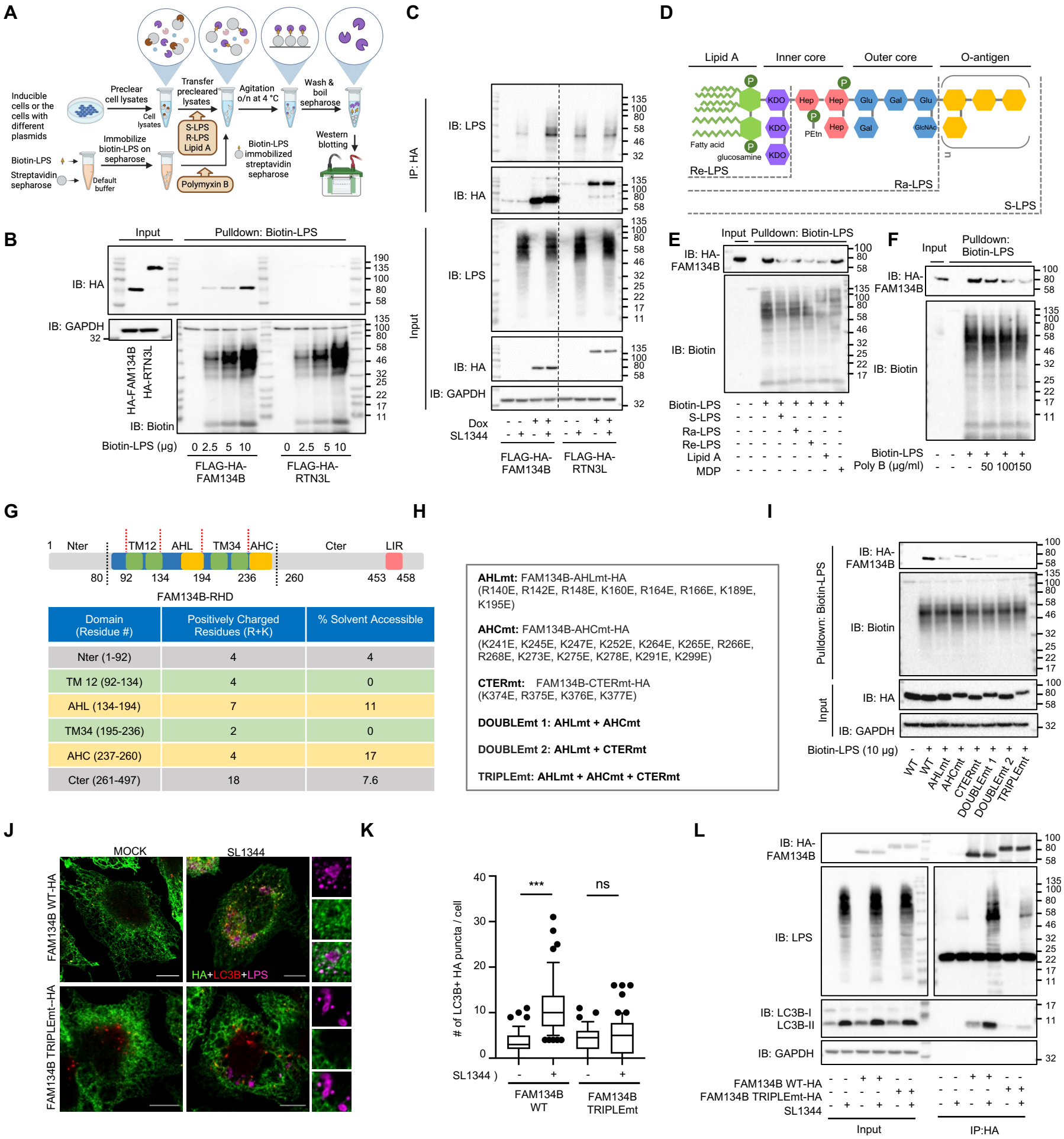

Domain (Residue #)	Positively Charged Residues (R+K)	% Solvent Accessible
Nter (1-92)	4	4
TM 12 (92-134)	4	0
AHL (134-194)	7	11
TM34 (195-236)	2	0
AHC (237-260)	4	17
Cter (261-497)	18	7.6

Figure 3 Cheng et al

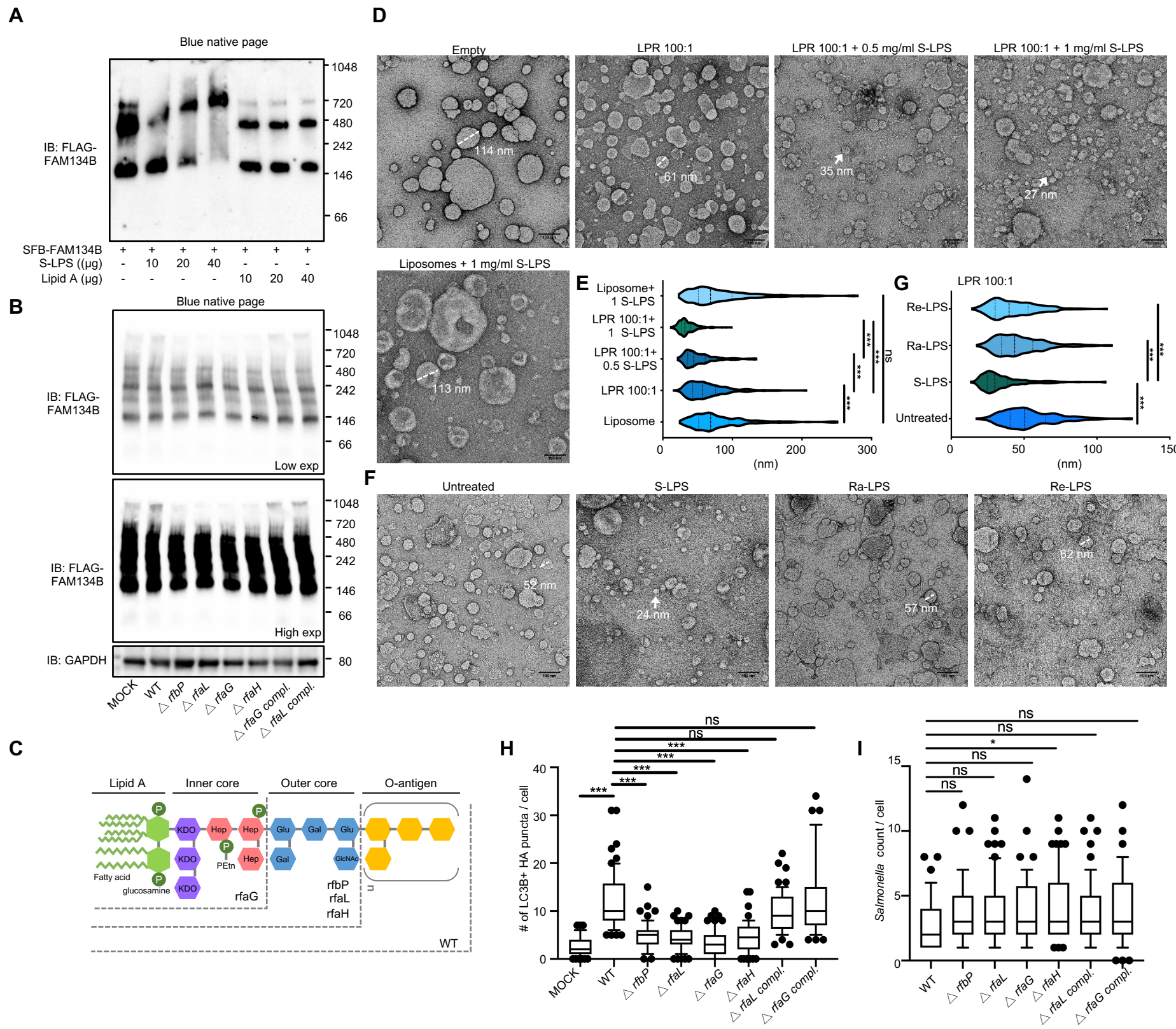

Figure 4 Cheng et al

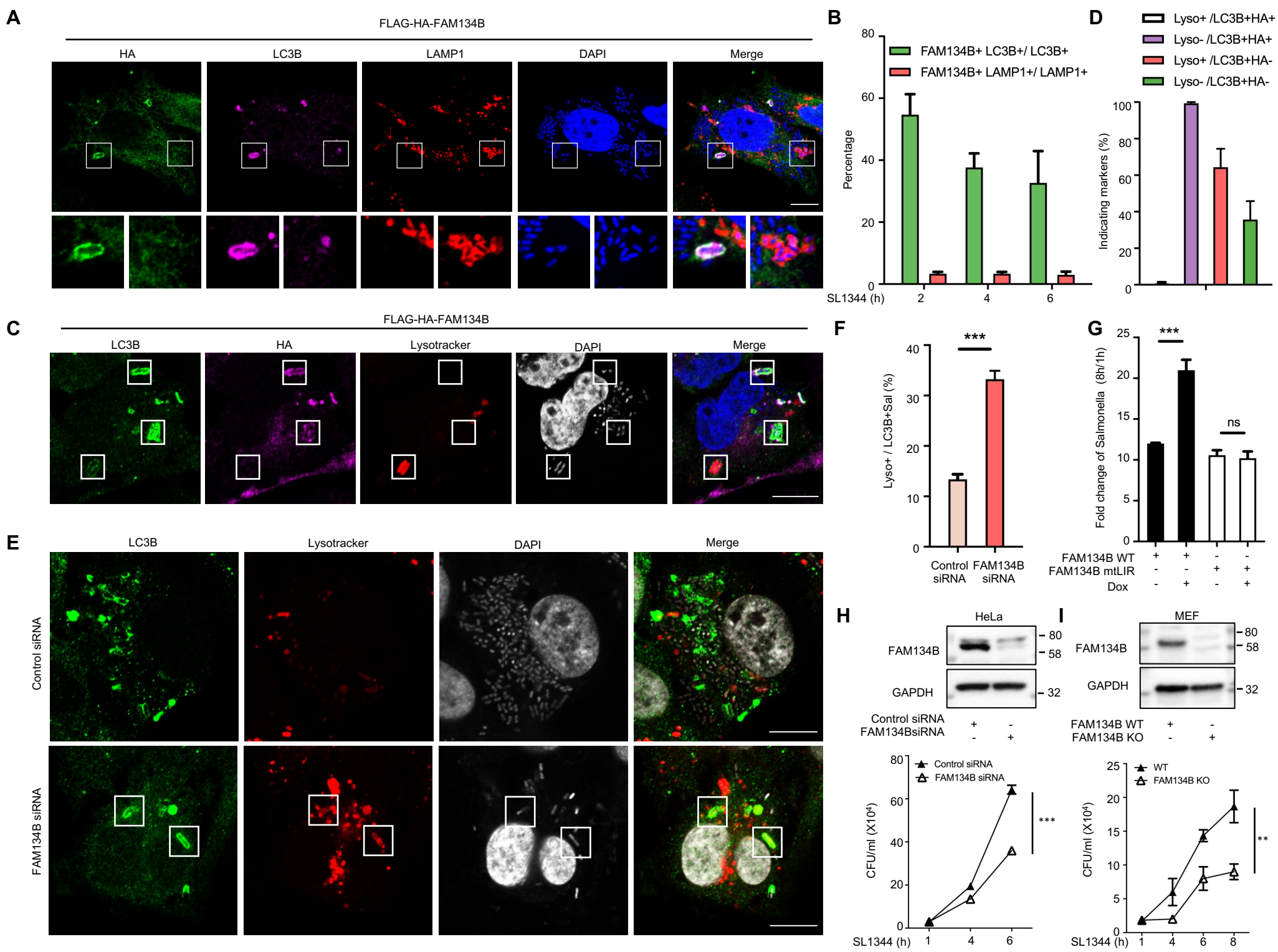

Figure 5 Cheng et al

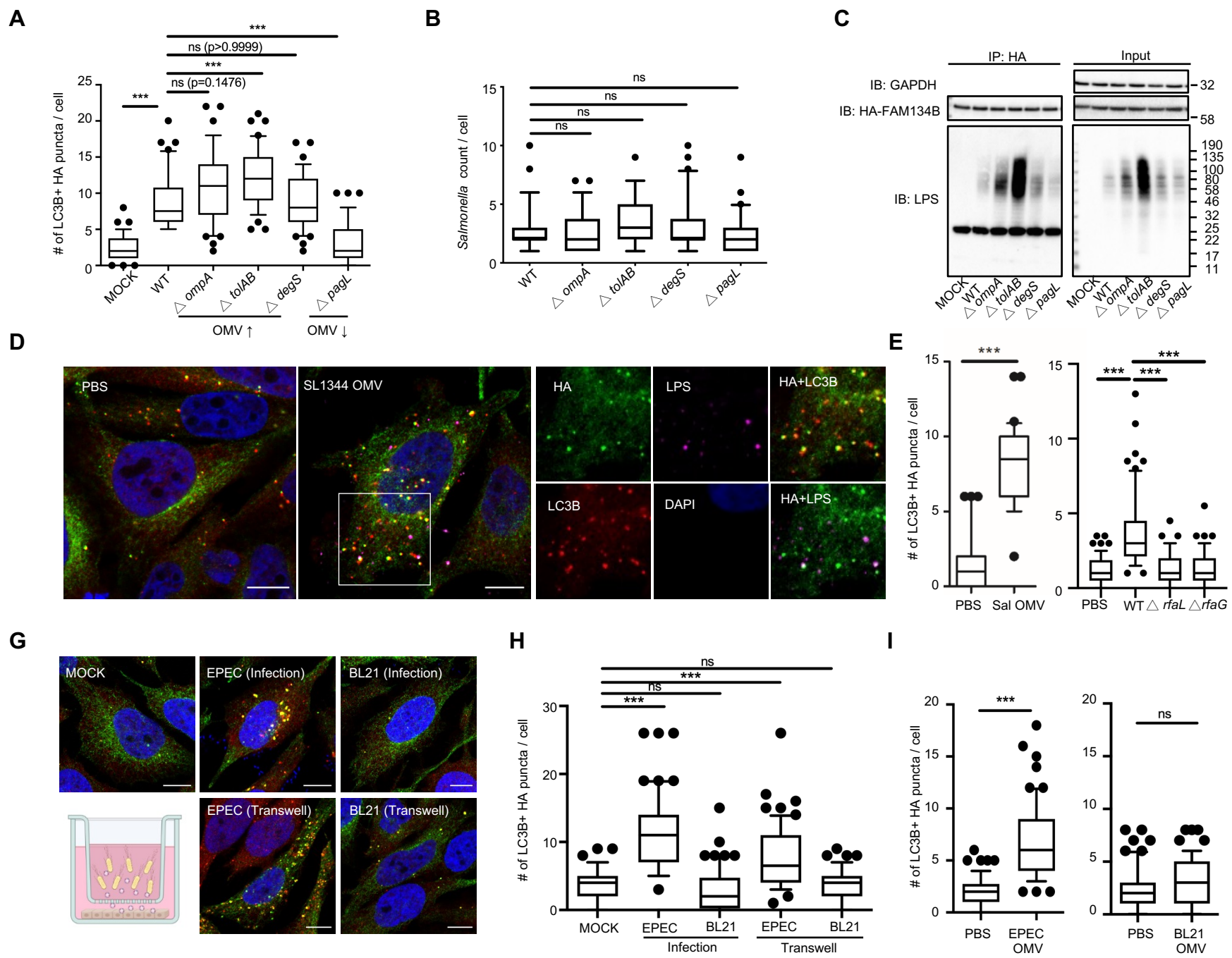

Supplementary information

Intracellular lipopolysaccharide regulates ER remodeling upon bacterial infection

Authors

Yi-Lin Cheng, João Mello-Vieira, Adriana Covarrubias-Pinto, Alexis Gonzalez, Santosh Kumar Kuncha, Chun Kew, Kaiyi Zhang, Muhammad Awais Afzal, Nour Diab, Sophia Borchert, Wenbo Chen, Timothy Chun Huang, Mathias Walter Hornef, Christian A. Hübner, Michael Hensel, Ivan Dikic

Figure S1

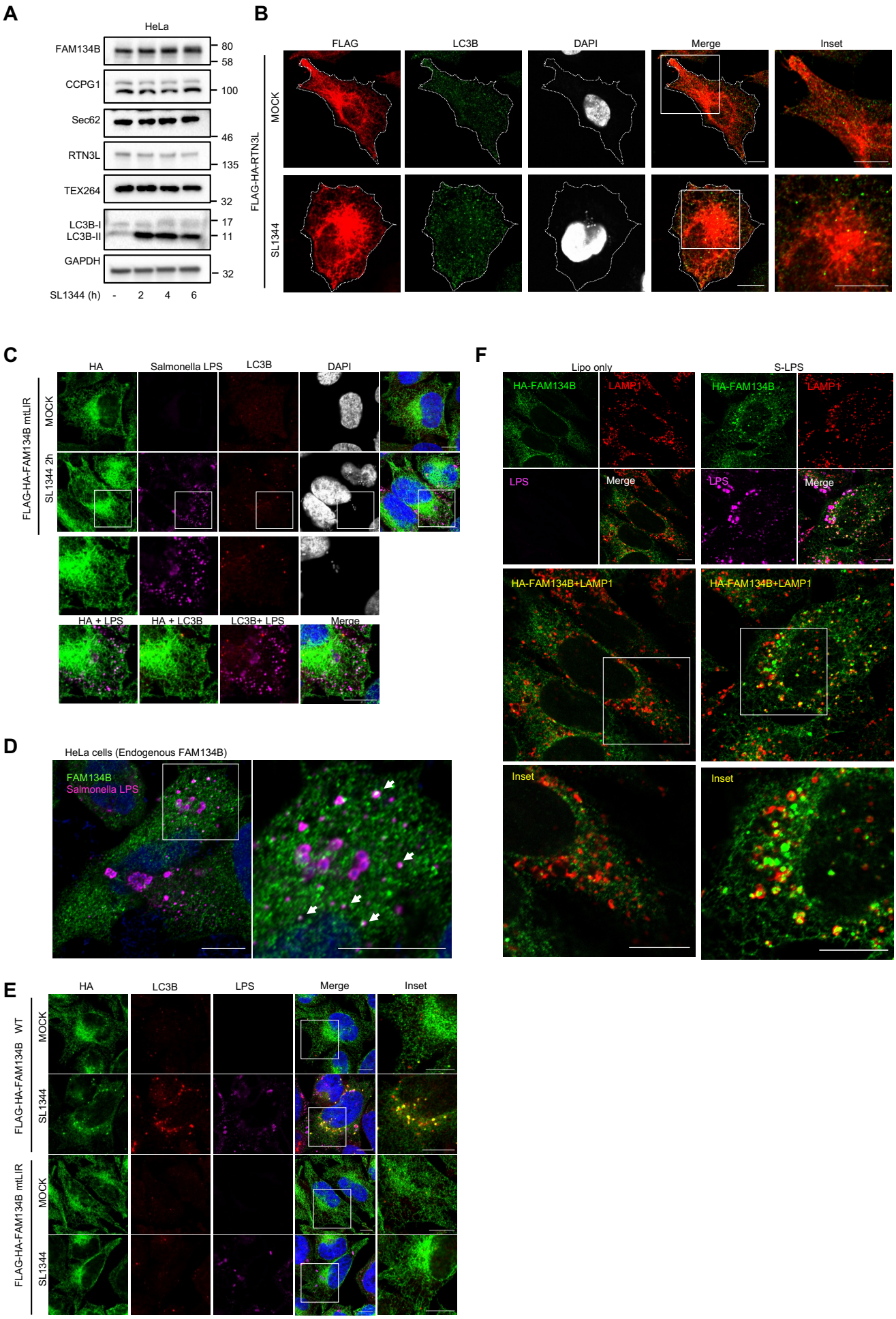
A
HeLa
FAM134B
CCPG1
Sec62
RTN3L
TEX264
LC3B-I
LC3B-II
GAPDH
80
58
100
46
135
32
17
11
32
SL1344 (h) - 2 4 6
B
FLAG
LC3B
DAPI
Merge
Inset
FLAG-HA-RTN3L
MOCK
SL1344
C
HA
Salmonella LPS
LC3B
DAPI
FLAG-HA-FAM134B mtLIR
MOCK
SL1344 2h
HA + LPS
HA + LC3B
LC3B+ LPS
Merge
D
HeLa cells (Endogenous FAM134B)
FAM134B
Salmonella LPS
E
HA
LC3B
LPS
Merge
Inset
FLAG-HA-FAM134B WT
MOCK
SL1344
FLAG-HA-FAM134B mtLIR
MOCK
SL1344
F
Lipo only
S-LPS
HA-FAM134B
LAMP1
LPS
Merge
HA-FAM134B+LAMP1
Inset

Figure S1. *Salmonella* infection mainly activates FAM134B-mediated ER fragmentation, related to Figure 1

(A) HeLa cells were infected with SL1344 for the indicated time points followed by analyzing the protein expression of indicated ER-phagy receptors, and LC3B by western blotting. GAPDH was used as an internal control of input.

(B) Immunofluorescence staining of FLAG and LC3B in HeLa TREx inducible cell lines expressing FLAG-HA-RTN3L, which were infected with SL1344 for 2 hr. DAPI was used for cell nuclear and bacterial DNA staining. Scale bar, 10 μm.

(C) Immunofluorescence staining of HA, *Salmonella* LPS, and LC3B in HeLa TREx inducible cell lines expressing LIR mutant (mtLIR) FLAG-HA-FAM134B infected with SL1344 for 2 hr. DAPI was used for cell nuclear and bacterial DNA staining. Scale bar, 10 μm.

(D) Immunofluorescence staining of FAM134B and *Salmonella* LPS in HeLa cells infected by SL1344 for 2 hr. Arrows indicate the puncta with colocalization of FAM134B and *Salmonella* LPS.

(E) Immunofluorescence staining of HA and LC3B in HeLa TREx inducible cell lines expressing wild type (WT) or mtLIR FLAG-HA-FAM134B infected with SL1344 for 2 hr. DAPI was used for cell nuclear and bacterial DNA staining. Scale bar, 10 μm.

(F) Immunofluorescence staining of HA, LAMP1, and *Salmonella* LPS in HeLa TREx inducible cell lines expressing FLAG-HA-FAM134B, which were transfected with 1 μg/ml *Salmonella* LPS for 18 hr by lipofectamine 2000. Lipo, lipofectamine only.

Figure S2

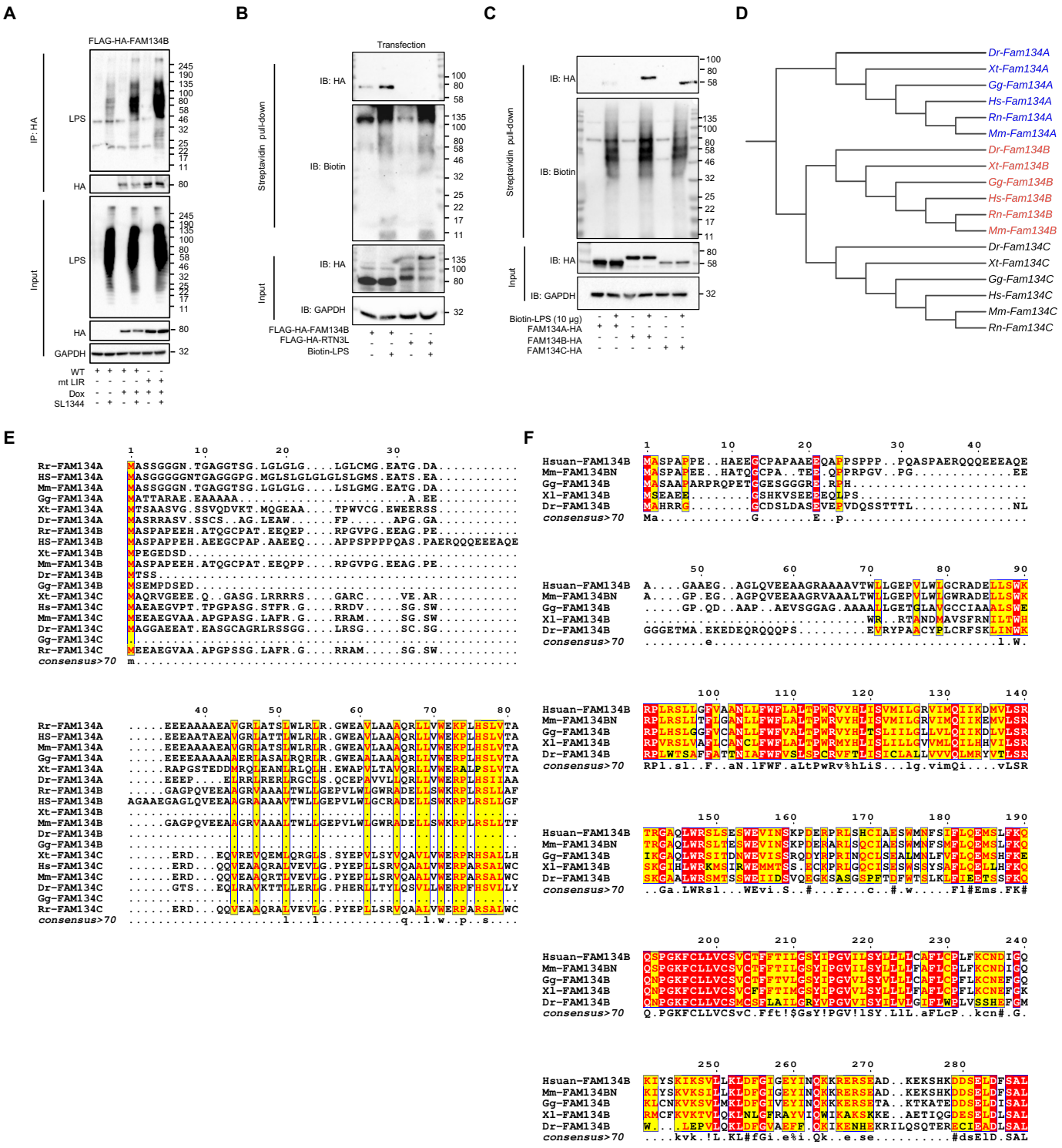

Figure S2. LPS bind to FAM134B and FAM134C, but not RTN3L and FAM134A, related to Figure 2

(A) Co-IP of LPS with HA in HeLa TREx inducible cell lines without Dox treatment or expressing FLAG-HA-FAM134B WT or FLAG-HA-FAM134B mtLIR with Dox treatment infected with SL1344 100 moi for 2 hr. GAPDH was used as an internal control of input.

(B) Streptavidin pulldown assays for determining the binding of the transfected biotin-conjugated *E. coli* O111:B4 LPS (10 μg) to HA-tagged FAM134B or RTN3L in FLAG-HA-FAM134B- or FLAG-HA-RTN3L-expressing HeLa TREx cell lines. GAPDH was used as an internal control of input.

(C) Streptavidin pulldown assays determining the binding of the biotin-conjugated *E. coli* O111:B4 LPS to HA-tagged FAM134A, FAM134B, or FAM134C in HA-FAM134A-, HA-FAM134B-, or HA-FAM134C-transfected HeLa cell lysates. GAPDH was used as an internal control of input.

(D-F) Phylogenetic tree of FAM134 proteins: Phylogenetic tree of FAM134A, B and C was generated by using ClustalW followed by analyzing the data through the iTOL server (https://itol.embl.de/). Representative sequences were derived from the FASTA for the following organism across phylum Chordata. Dr: *Danio rerio*, Xt: *Xenopus tropicalis*, Gg: *Gallu gallus*, Rn: *Rattus norvegicus*, Mm: *Mus musculus* and Hs: *Homo sapiens*

Figure S3

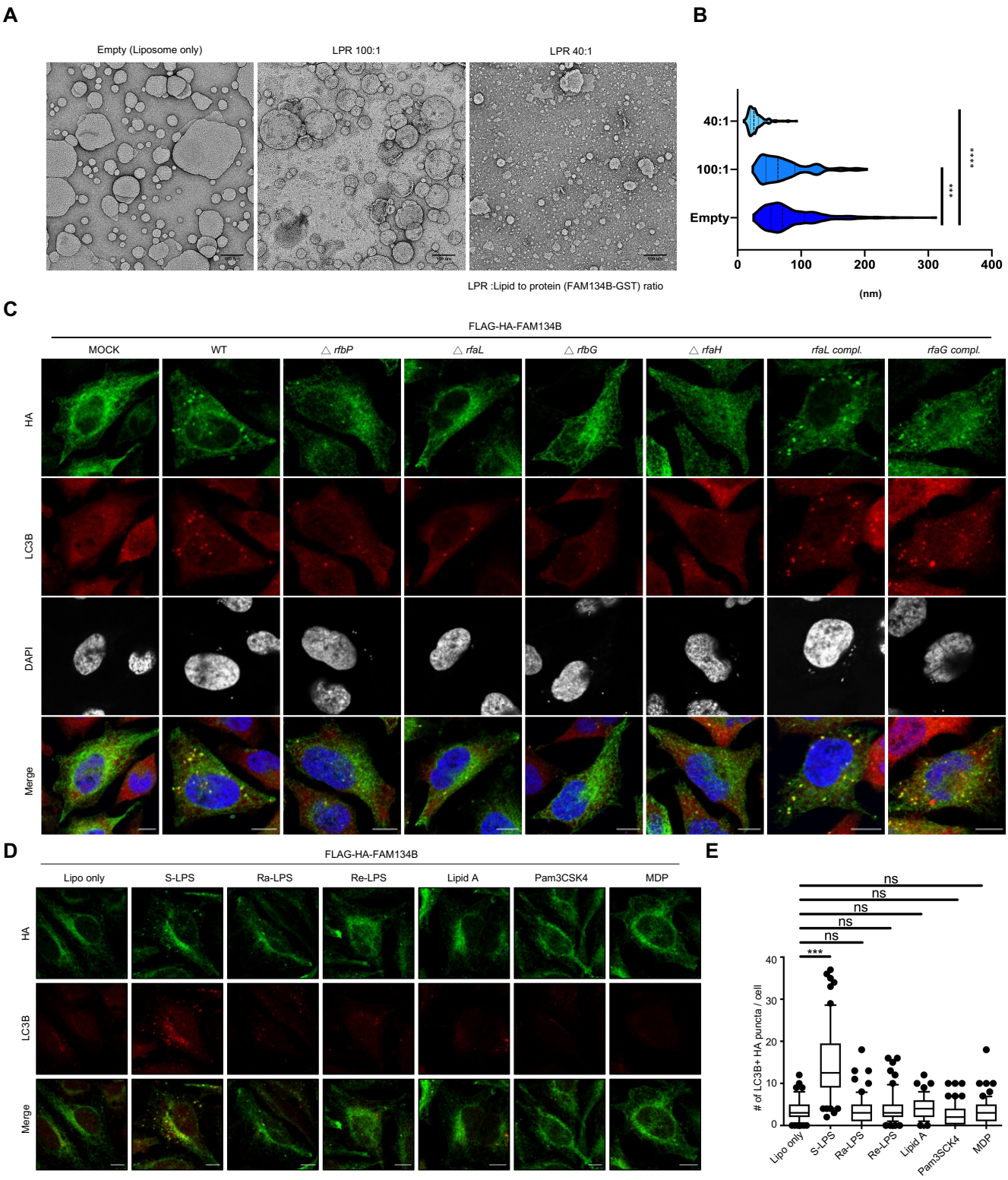

Figure S3. S-LPS trigger membrane fragmentation, related to Figure 3

(A-B) Representative images (A) of remodeled proteoliposomes (scale bars, 100 nm) taken from nsTEM. Empty liposomes (Empty) were added to FAM134B-GST recombinant protein at a lipid to protein ratio (LPR) 100:1 (LPR 100:1) or 40:1 (LPR 40:1). The size distributions (n=300 each) from nsTEM images were measured and presented by violin plots, showing a central boxplot (black lines indicate median with interquartile range) with mirrored histograms on both sides (B). Differences

were statistically analyzed by one-way ANOVA and Tukey's multiple comparison test. ***$p < 0.001$. ns, not significant.

(C) Immunofluorescence of HA, *Salmonella* LPS, and LC3B in HeLa TREx inducible cell line expressing FLAG-HA-FAM134B were infected with NCTC12023 WT or LPS O-Ag mutant (Δ) and complemented (compl.) strains for 2 hr. DAPI staining was used for cell nuclear and bacterial DNA staining. Scale bar, 10 μm.

(D-E) Immunofluorescence staining of HA and LC3B in HeLa TREx inducible cell line expressing FLAG-HA-FAM134B, transfected with 1 μg/ml S-LPS, Ra-LPS, Re-LPS, Lipid A, Pam3CSK4, and MDP for 18 hr by lipofectamine 2000 (D). Lipo, lipofectamine only. DAPI was used for cell nuclear DNA staining. Scale bar, 10 μm. Quantification of LC3B-positive HA-FAM134B puncta per cell (E). Solid bars of boxes indicate the medians. Boxes represent interquartile range from 25th to 75th percentile, and whiskers indicate 10th to 90th percentile. Differences were statistically analyzed by one-way ANOVA and Tukey's multiple comparison test. ***$p < 0.001$. ns, not significant. Data were collected 60 cells from three independent biological replicates.

Figure S4

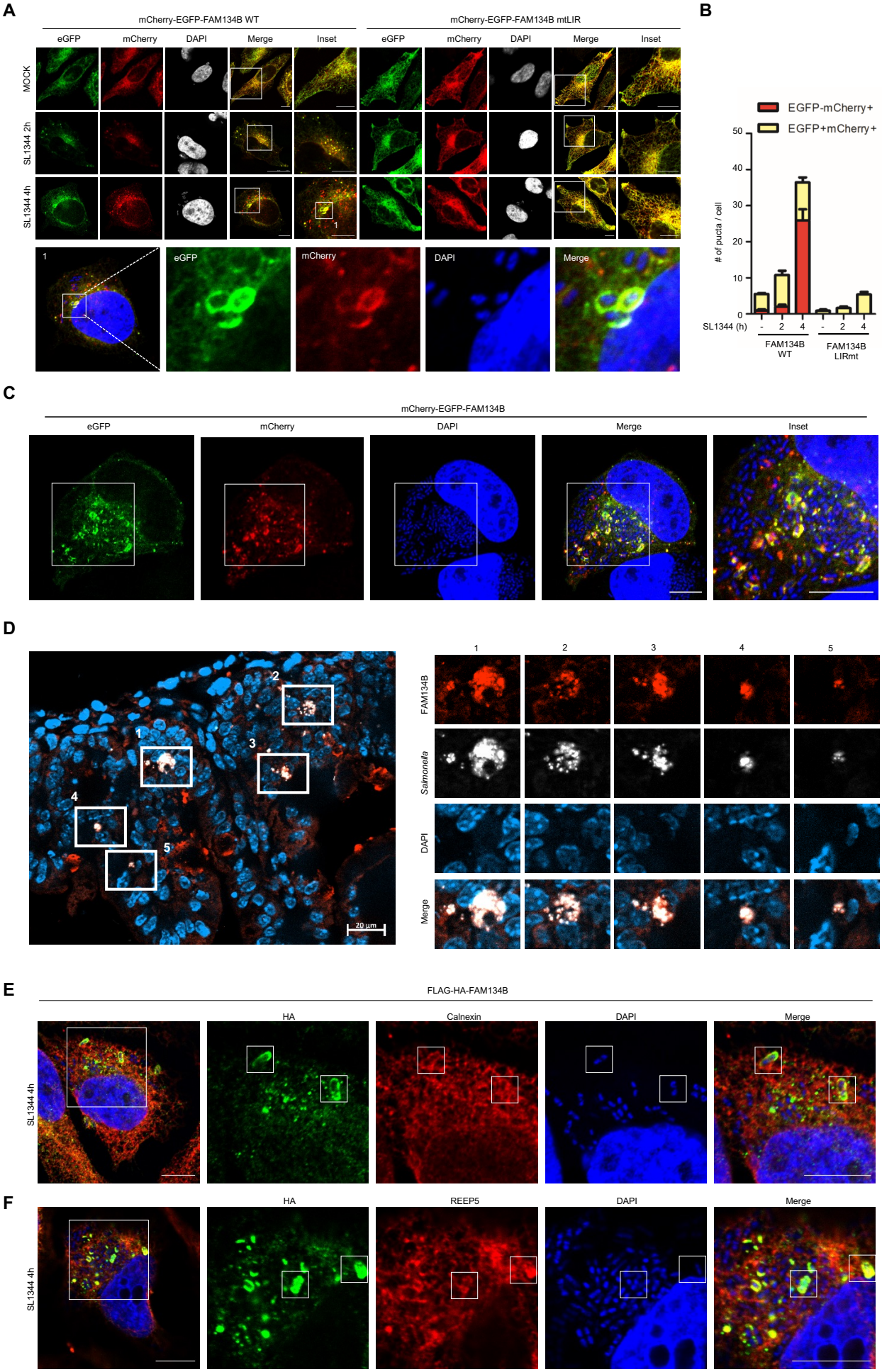
A
mCherry-EGFP-FAM134B WT
mCherry-EGFP-FAM134B mtLIR
eGFP
mCherry
DAPI
Merge
Inset
MOCK
SL1344 2h
SL1344 4h
B
EGFP-mCherry+
EGFP+mCherry+
# of pucta / cell
SL1344 (h)
FAM134B WT
FAM134B LIRmt
C
mCherry-EGFP-FAM134B
D
FAM134B
Salmonella
20 µm
E
FLAG-HA-FAM134B
HA
Calnexin
F
REEP5

Figure S4. *Salmonella* activates FAM134B-mediated ER-phagy and ER fragmentation, forming bacteria-containing vacuoles positive for FAM134B and ER markers, related to Figure 4

(A-C) HeLa TREx inducible cell lines expressing mCherry-eGFP-FAM134B WT or mCherry-eGFP-FAM134B mtLIR were infected with SL1344 for 2 hr or 4hr (A). The inset of square 1 showed the *Salmonella* surrounded by mCherry and eGFP double positive-FAM134B (A). Quantification of mCherry-positive and eGFP-negative puncta (red) and double-positive (yellow) puncta per cell (B). The cell with hyperproliferating *Salmonella* showed bacteria surrounded by mCherry and eGFP double positive-FAM134B (C). DAPI staining was used for cell nuclear and bacterial DNA staining. Scale bar, 10 μm.

(D) Immunofluorescence staining of FAM134B (red) in *Salmonella*-infected intestinal tissue section obtained at day 4 post-infection. *Salmonella* GFP staining was used for detecting GFP plasmid carried by *Salmonella* (white). DAPI was used for nuclear DNA staining. Scale bar, 20 μm.

(E-F) Immunofluorescence staining of HA and Calnexin (E) or REEP5 (F) in HeLa TREx inducible cell lines expressing FLAG-HA-FAM134B, which were infected with SL1344 for 4 hr. DAPI was used for nuclear and bacterial DNA staining. Scale bar, 10 μm.

Figure S5

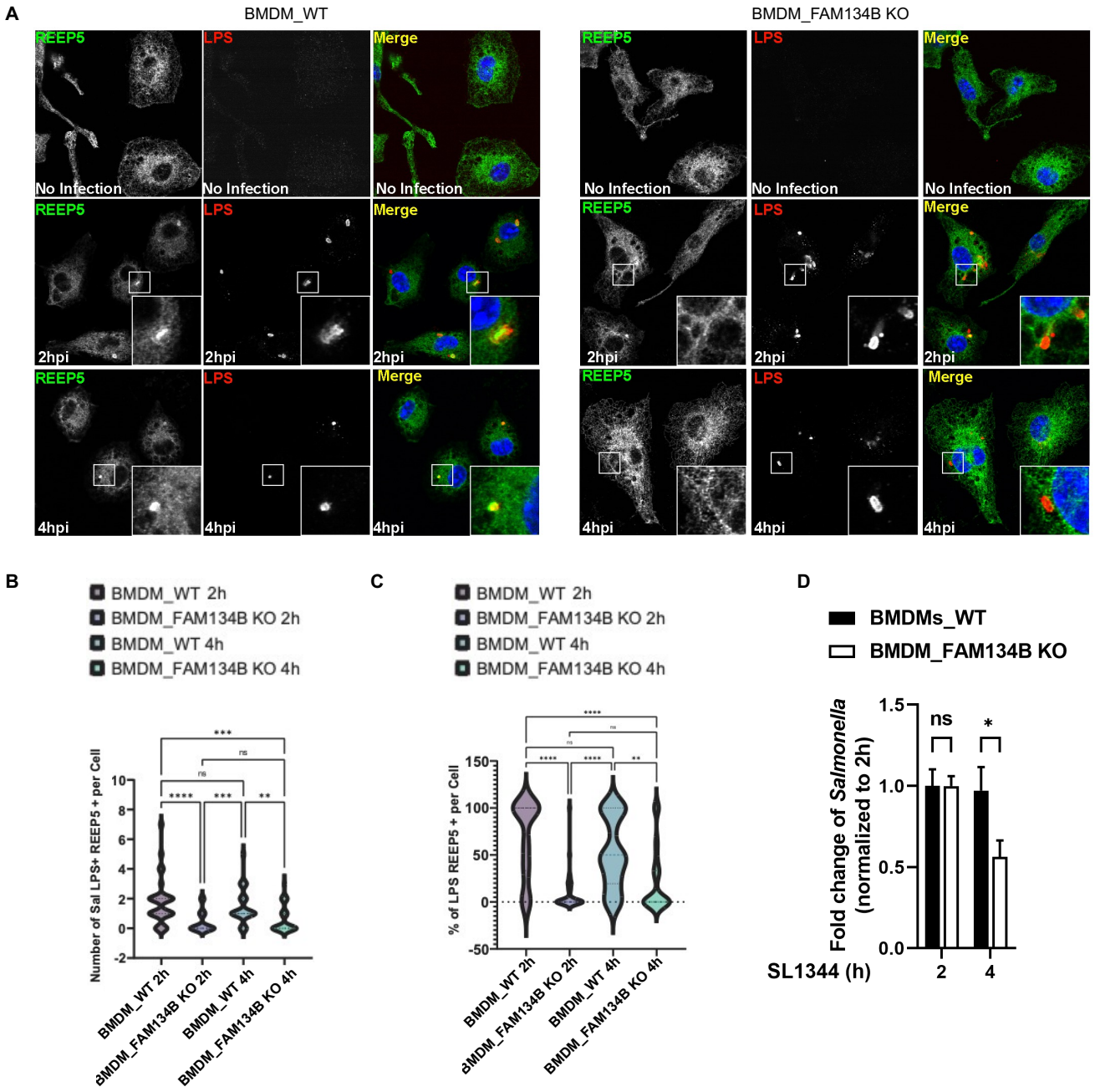

Figure S5., FAM134B promotes ER-surrounded *Salmonella*-containing vacuoles formation and bacterial growth in BMDM, related to Figure 4.

(A-C) Immunofluorescence staining of REEP5 (ER marker) and *Salmonella* LPS in WT BMDMs or FAM134B KO BMDMs, which were infected with SL1344 for 2hr (2hpi) or 4 hr (4hpi). *Salmonella* LPS staining was used to indicate bacteria. Quantification of immunofluorescence analysis represented as (B) number of vacuoles stained with LPS and REEP5 per cell, (C) percentage of *Salmonella* (LPS) positive to REEP5 from total *Salmonella*. Data are mean ± sem of the number of ER-positive *Salmonella*-containing vacuoles (LPS$^+$ and REEP+) and % of these vacuoles (LPS$^+$ and REEP5$^+$) from total *Salmonella* (LPS$^+$) per cell (2 h: $n = 34$ for the FAM134B KO, $n = 30$ for the WT and 4h: $n = 36$ for FAM134B KO and $n = 29$, Kruskal–Wallis/Dunn's post-test). **p<0.01, **p<0.0001, ****p<0.0001 ns, not significant.

(D) Colony-forming assay was performed to quantify the bacteria count in WT or FAM134B KO BMDMs followed by infection with SL1344 10 moi for the indicated timepoints. The growth fold change at 4 hr was normalized to 2 hr, error bars represent standard error of the mean. *$p<0.05$. Data were collected from three pairs of WT and FAM134B KO mice.

Figure S6

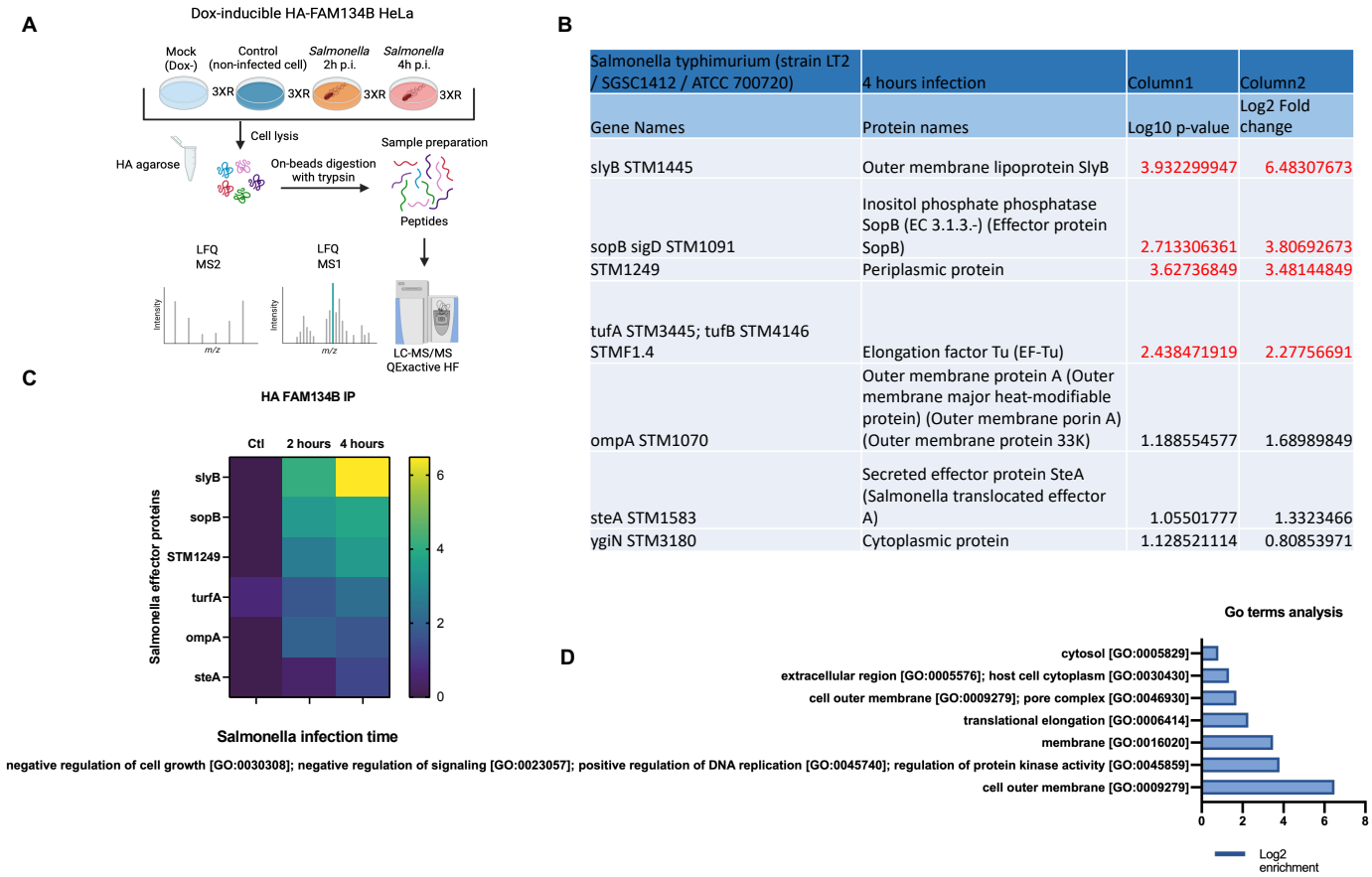

Salmonella typhimurium (strain LT2 / SGSC1412 / ATCC 700720)	4 hours infection	Column1	Column2
Gene Names	Protein names	Log10 p-value	Log2 Fold change
slyB STM1445	Outer membrane lipoprotein SlyB	3.932299947	6.48307673
sopB sigD STM1091	Inositol phosphate phosphatase SopB (EC 3.1.3.-) (Effector protein SopB)	2.713306361	3.80692673
STM1249	Periplasmic protein	3.62736849	3.48144849
tufA STM3445; tufB STM4146 STMF1.4	Elongation factor Tu (EF-Tu)	2.438471919	2.27756691
ompA STM1070	Outer membrane protein A (Outer membrane major heat-modifiable protein) (Outer membrane porin A) (Outer membrane protein 33K)	1.188554577	1.68989849
steA STM1583	Secreted effector protein SteA (Salmonella translocated effector A)	1.05501777	1.3323466
ygiN STM3180	Cytoplasmic protein	1.128521114	0.80853971

Figure S6. FAM134B-interacting *Salmonella* proteins obtained from the interactome of FAM134B, related to Figure 4

(A) MS workflow for the analysis of HA–FAM134B co-immunoprecipitated from cell lysates following *Salmonella* infection (2 and 4h) and Control (non-infected cells, blue) or from mock (HA empty, light blue). HF, Q Exactive HF (Ultra-High-Field Orbitrap) mass spectrometer; LFQ, label free quantification; 3xR 3 biological replicates.

(B) Table showing the list of *Salmonella* effectors found in the HA-FAM134B co-immunoprecipitation. Significant and enriched hits are colored in red (significant values were $\log_2$ enrichment > 1.0 and $-\log_{10}$ p value > 1.3). Data are means ± s.d. of $n = 3$ independent experiments.

(C) Heat map comparing the interaction of Salmonella effector proteins with WT FAM134B after 2 or 4 hours of infections (immuno-isolated using HA beads). Interaction partners with $\log_2$ enrichment > 1.0 and $-\log_{10}$ p value > 1.3 were plotted. $n = 3$ independent experiments, one-tailed unpaired Student's test.

(D) Annotation enrichment analysis of the *Salmonella* effector proteins interacting with FAM134B. Bars represent significantly enriched gene ontology biological process (GOBP), gene ontology cellular component (GOCC) for the identified *Salmonella* proteins.

Figure S7

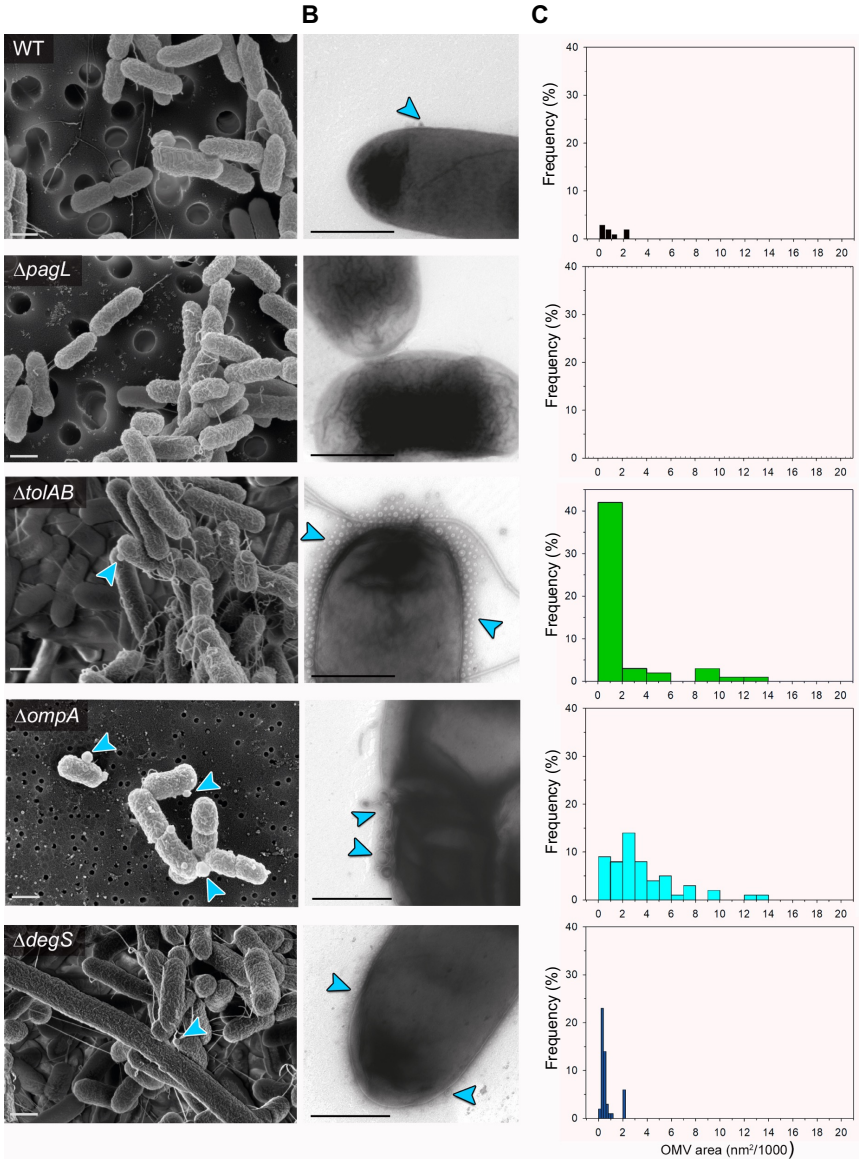
A
B
C
WT
ΔpagL
ΔtolAB
ΔompA
ΔdegS
Frequency (%)
OMV area (nm²/1000)

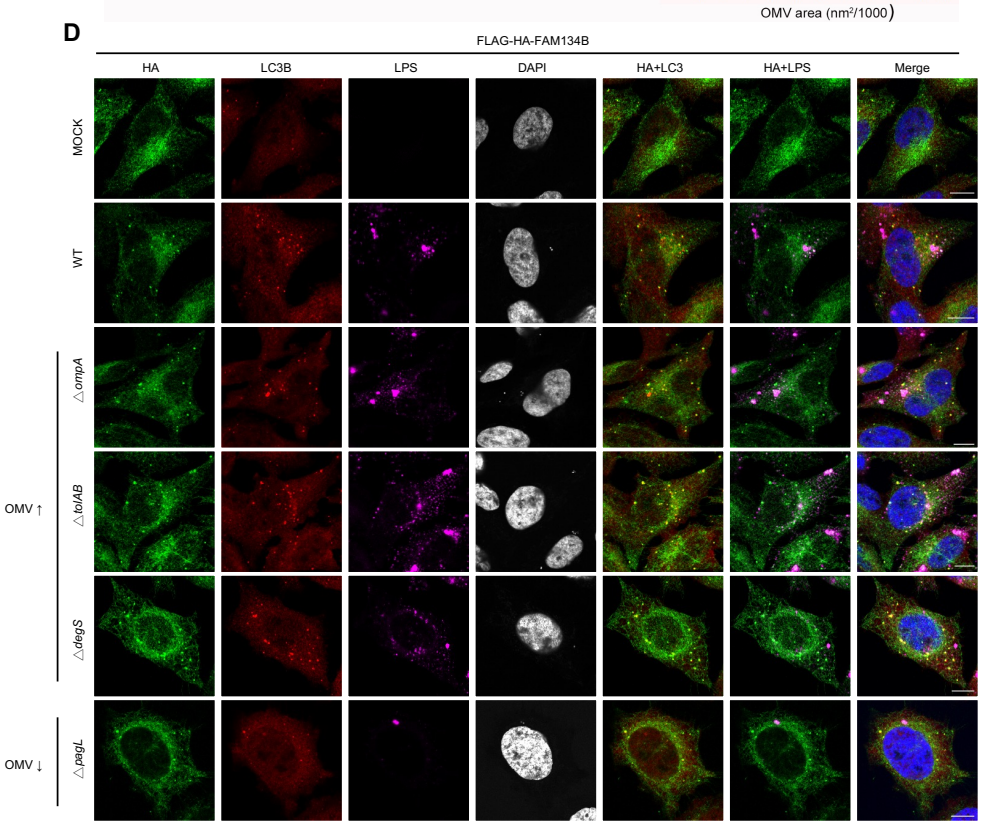
D
FLAG-HA-FAM134B
HA
LC3B
LPS
DAPI
HA+LC3
HA+LPS
Merge
MOCK
WT
△ompA
△tolAB
△degS
△pagL
OMV ↑
OMV ↓

Figure S7. Formation of OMV by various *Salmonella* strains and OMV size distribution, related to Figure 5.

(A-C) STM WT, or mutant strains deficient in *pagL*, *tolAB*, *ompA*, or *degS* were grown on filter paper placed on LB agar (A), or overnight on LB agar to allow formation of colonies (B). (A) Cells were fixed, dehydrated, and coated with 10 nm gold and prepared for SEM imaging on JEOL IT-200 and Zeiss Auriga systems. (B) For TEM micrographs, samples were prepared using negative stain. The study was performed as triplicates, 20 bacteria per strain were recorded. Cultures were grown statically on filter papers on LB agar. The experiment was performed as duplicates, at least ten images were generated from each strain. Representative OMV are indicated by arrowheads. Scale bars, 500 nm. (C) Size distribution of OMV was determined using morphometric analyses in FIJI. For this, the areas of OMV of at least six bacteria per strains were quantified and the frequency of various OMV size populations was plotted as histogram. The WT strain possessed OMVs of 918 nm^2 on average, and OMVs up to 2,000 nm^2 were also detected. No vesicles could be detected for Δ*pagL*. The other three mutant strains showed increased production of OMVs compared to WT strain, and the average sizes of OMVs were 1,611 nm^2 in Δ*tolAB*, 3,153 nm^2 in Δ*ompA*, and 590 nm^2 in Δ*degS*.

(D) Immunofluorescence staining of HA, *Salmonella* LPS, and LC3B in cells infected with different mutant strains, including Δ*ompA*, Δ*tolAB*, and Δ*degS*, and Δ*pagL* strains. DAPI was used for cell nuclear and bacterial DNA staining. Scale bar, 10 μm. Quantification of LC3B-positive HA-FAM134B puncta and *Salmonella* count per cell are shown in Figure 5A and 5B.

Figure S8

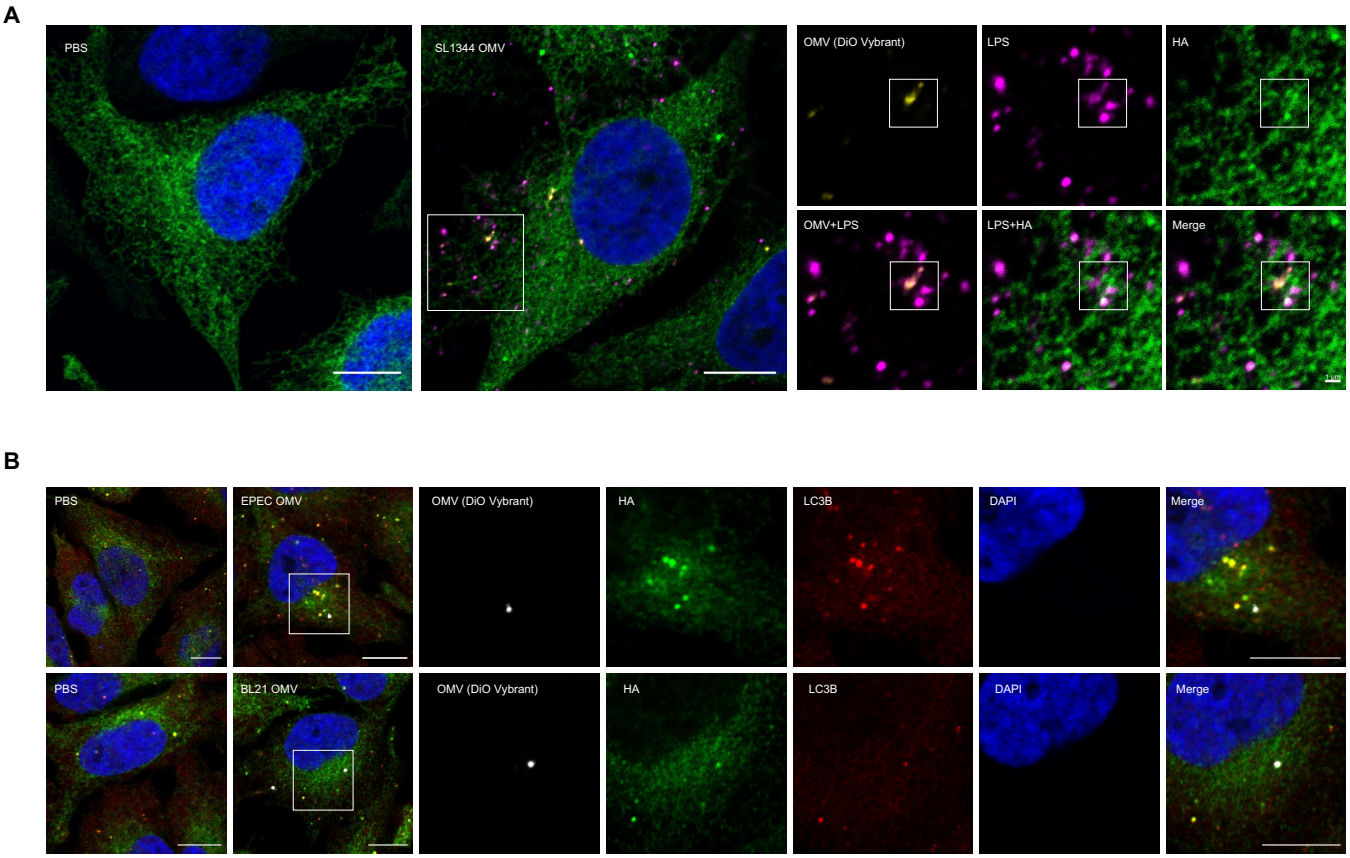

Figure S8. FAM134B colocalized with LPS, which is not associated with OMVs, related to Figure 5

(A) *Salmonella* OMVs were stained by DiO Vybrant dye first, then applied to HeLa TREx inducible cell lines expressing FLAG-HA-FAM134B for 4 hr followed by Immunofluorescence staining of HA and *Salmonella* LPS. DAPI was used for nuclear DNA staining. Scale bar, 10 μm.
(B) EPEC or BL21 OMVs were stained by DiO Vybrant dye first, then applied to HeLa TREx inducible cell lines expressing FLAG-HA-FAM134B for 4 hr followed by Immunofluorescence staining of HA and LC3B.

METHOD DETAILS

Mouse model for *S.* Typhimurium infection

Salmonella enterica subsp. enterica serovar Typhimurium ATCC14028 (NCTC12023) carrying a green fluorescent protein (GFP) expression plasmid (pGFP, AmpR, kindly provided by Brendan Cormack, Stanford, USA) were cultured in Luria Bertani (LB) broth overnight at 37°C. The overnight culture was diluted 1:10 in fresh LB and incubated at 37°C until reaching the logarithmic phase (OD600 approximately 0.5). Bacteria were washed and adjusted to OD600 0.55–0.60 containing approximately 1.5–2.0×10^8 CFU/ml. One-day-old C57BL/6 animals were infected orally with 10^2 CFU *S*. Typhimurium in a volume of 1 µl PBS. The administered inoculum was confirmed by serial dilution and plating. At day 4 post-infection, the small intestine tissue was collected and fixed in 4% PFA.

HA-FAM134B interactome analysis in cells infected with *Salmonella* and sample preparation for MS

HeLa TREx cells were induced with doxycycline to express HA-FLAG FAM134B. After 16 h, cells were infected with *Salmonella* for 2 and 4 hours. After the infection with *Salmonella*, cells were lysed with 1% Triton X-100 in lysis buffer (50 mM Tris-HCl pH 7.5, 150 mM NaCl, 0.5 mM EDTA, Roche EDTA-free protease inhibitor cocktail and NEM), followed by incubation with HA-beads (Sigma-Aldrich) overnight at 4 °C on a rotating platform. Protein-bound beads were washed three times with lysis buffer and three times in the same buffer without detergents before the elution. Samples were eluted with 25 µl SDC buffer (2% sodium deoxycholate and 50 mM Tris-HCl pH 8.5) and heated to 95 °C for 5 min. Additionally, 25 ul of 50 mM Tris-HCl pH 8.5 containing 1 mM TCEP, 4 mM chloroacetamide were added to the samples in order to alkylate and reduce the proteins and incubated to 95 °C for 5 min. We then added 500 ng trypsin in 25 µl 50 mM Tris-HCl (pH 8.5) to each sample and incubated overnight at 37 °C. The reaction was stopped with 150 µl of 1% TFA in isopropanol. Peptides were cleaned up using SDB-RPS stage tips (Sigma-Aldrich). After one wash with 1% TFA in isopropanol and one wash with 0.2% TFA in water, peptides were eluted in 80% acetonitrile plus 1.25% ammonia. Eluted peptides were dried and processed for LC–MS.

LC–MS analysis

Dried peptides were resolved in 2% acetonitrile containing 0.1% TFA and loaded to the 35-cm, 75-µm ID fused-silica column, which packed in house with 1.9-µm C18 particles (Reprosil pur, Dr. Maisch), then analyzed on a QExactive HF mass spectrometer coupled to an easy nLC 1200 (Thermo Fisher Scientific). An integrated column oven (Sonation) was used to maintain the column at 50 °C. Peptides were eluted using a non-linear gradient of 4–28% acetonitrile over 45 min followed by sprayed into the mass spectrometer with a nanoFlex ion source (Thermo Fisher Scientific). Full-scan MS spectra (300–1,650 *m*/*z*) were acquired in a profile mode with resolution of 60,000 at *m*/*z* 200, a maximum injection time of 20 ms and an automatic gain control (AGC) target value of 3 × 10^6. Using a 1.4-Th window, up to 15 of the most intense peptides per full scan were isolated for fragmentation by higher energy collisional dissociation with normalized collision energy of 28.

MS/MS spectra were acquired at a resolution of 30,000, a maximum injection time of 45 ms and an AGC target value of 1×10^5 in centroid mode. Ions with unassigned charge states, single charged ions, and ions with a charge state of more than four were excluded for fragmentation. To minimize the acquisition of fragment spectra representing already acquired precursors, dynamic exclusion was set to 20 s.

MS data processing

MaxQuant (v1.6.17.0) was used to process MS raw data. Acquired spectra were searched against the human 'one sequence per gene' database (Taxonomy ID 9606) downloaded from UniProt (12 March 2020; 20,531 sequences), and a collection of 244 common contaminants ('contaminants.fasta' provided with MaxQuant v1.6.17.0) using the Andromeda search engine integrated into MaxQuant (v1.6.17.0). Protein identifications were obtained by filtering at false discovery rates below 1% for both peptide spectrum matches and proteins using a target–decoy strategy (Elias and Gygi, 2007). Protein quantification and data normalization relied on the MaxLFQ algorithm (Cox et al., 2014). The MS proteomics data have been deposited to the ProteomeXchange Consortium through the PRIDE partner repository (Perez-Riverol et al., 2022) with the dataset identifiers PXD053709 (Fig. S6). For protein assignment, the UniProt human database v2019 including a list of common contaminants was introduced to correlate with spectra. Tryptic specifications and default settings for mass tolerances in MS and MS/MS spectra were applied for searches. The match-between-run feature was used with a time window of 1 min. For further analysis, Perseus (v2.0.7.0) was applied to obtain the proteins with significant changed between groups after filtering contaminants, reverse entries, and proteins that were only identified by a modified peptide.

Establishment of mCherry-EGFP-FAM134B inducible cell lines

mCherry-EGFP-FAM134B WT and mCherry-EGFP-FAM134B mtLIR constructs were cloned into pcDNA5/FRT/TO vector by GATEWAY technology, followed by co-transfection with recombinase pOG44 into Flp-In HeLa TREx cells. Then, 400 µg/ml hygromycin and 15 µg/ml blasticidin were treated for selection and maintenance of stable cells. Induction was performed with 2 µg/ml doxycycline for 24 hr.

Analysis of OMV production by SEM

For ultrastructural analyses, liquid cultures were incubated overnight. Circles of Whatman Nucleopore membrane filters (pore size 0.1 µm) were punched out of using a biopsy punch. The filters were placed shiny side up on an agar plate, and 2 µl of bacterial cultures were transferred to the center of filters. The agar plates were incubated overnight at 37 °C. The filters were fixed for 15 min in a 1.5 ml reaction tube containing 2.5% GA in PBS. The fixative was removed and washed three times with PBS. An increasing EtOH series was used to dehydrate the samples. This involved 10%, 30%, 50%, 70%, 90% EtOH for 10 min each, with the last three dilution levels

applied twice. Subsequently, the samples were incubated in 100% EtOH for 15 min and critical point drying was performed. After the samples were glued onto SEM stubs, they were coated with a 10 nm thick gold layer in order to inhibit charging during microscopy. Afterwards, the samples were imaged using a JEOL IT-200 for overview images, and with a Zeiss Auriga 60 for high-resolution images.

Analysis of OMV production using negative stain TEM

For high-resolution ultrastructural analyses, *Salmonella* cultures were grown on agar plates, then bacterial material was picked up with an inoculation loop and resuspended in 500 µl PBS. Here, the samples were carefully inverted to inhibit detachment of OMVs. Then, 5 µl of the bacterial suspension was transferred to a glow-discharged EM copper slot grid with Formvar charcoal coating and the cells were allowed to adhere for 5 min. The suspension was carefully removed with a filter paper and subsequently washed three times with 5 µl MilliQ. For negative stain, 1% uranyl acetate (UA) was applied to the grid for 1 min, and the excess UA was then removed with a filter paper. Afterwards, the samples were imaged by the Zeiss LEO912 and the JEOL JEM 2100Plus.

REFERENCES

Cox, J., Hein, M.Y., Luber, C.A., Paron, I., Nagaraj, N., and Mann, M. (2014). Accurate proteome-wide label-free quantification by delayed normalization and maximal peptide ratio extraction, termed MaxLFQ. Mol Cell Proteomics *13*, 2513-2526. 10.1074/mcp.M113.031591.

Elias, J.E., and Gygi, S.P. (2007). Target-decoy search strategy for increased confidence in large-scale protein identifications by mass spectrometry. Nat Methods *4*, 207-214. 10.1038/nmeth1019.

Perez-Riverol, Y., Bai, J., Bandla, C., Garcia-Seisdedos, D., Hewapathirana, S., Kamatchinathan, S., Kundu, D.J., Prakash, A., Frericks-Zipper, A., Eisenacher, M., et al. (2022). The PRIDE database resources in 2022: a hub for mass spectrometry-based proteomics evidences. Nucleic Acids Res *50*, D543-D552. 10.1093/nar/gkab1038.

KEY RESOURCES TABLE

Intracellular lipopolysaccharide regulates ER remodeling upon bacterial infection

Authors

Yi-Lin Cheng, João Mello-Vieira, Adriana Covarrubias-Pinto, Alexis Gonzalez, Santosh Kumar Kuncha, Chun Kew, Kaiyi Zhang, Muhammad Awais Afzal, Nour Diab, Sophia Borchert, Wenbo Chen, Timothy Chun Huang, Mathias Walter Hornef, Christian A. Hübner, Michael Hensel, Ivan Dikic

KEY RESOURCES TABLE

REAGENT or RESOURCE	SOURCE	IDENTIFIER
Antibodies		
HA	Roche	Cat# 11867423001; RRID:AB_390918
GAPDH	Cell signaling	Cat# 2118 RRID:AB_561053
Salmonella LPS	Abcam	Cat# ab8274 RRID:AB_306423
LC3B	MBL Life Science	Cat# PM036 RRID:AB_2274121
LC3B	MBL Life Science	Cat# M152-3 RRID:AB_1279144
Biotin	Santa Cruz	Cat# sc-101339 RRID:AB_1119609
FLAG	Sigma Aldrich	Cat# F3165 RRID:AB_259529
LAMP1	Abcam	Cat# ab24170 RRID:AB_775978
FAM134B	Proteintech	Cat# 21537-1-AP RRID:AB__2878879
CCPG1	Polyclonal rabbit, affinity purified with N-term peptide, gift from Simon Wilkinson	N/A
Sec62	Novusbio	Cat# NBP1-84045 RRID:AB_11037283
RTN3L	TebuBio	Cat# PA2256 RRID:AB_2665372
TEX264	Novus	Cat# NBP1-89866 RRID:AB_11009420
Calnexin	Abcam	Cat# ab22595 RRID:AB_2069006
REEP5	Santa Cruz	Cat# sc-393508
GAPDH	Cell signaling	Cat#2118S, RRID: AB_561053
GFP (for Salmonella-GFP)	Abcam	Cat#ab13970 RRID:AB_300798
Chemicals		
Biotinylated ultrapure LPS from *E. coli* 0111:B4	InvivoGen	Cat# tlrl-lpsbiot
LPS from *Salmonella enterica* serotype typhimurium	Sigma-Aldrich	Cat# L2262

LPS (rough strains) from *Salmonella enterica* serotype typhimurium TV119 (Ra mutant)	Sigma-Aldrich	Cat# L6016
LPS (rough strains) from *Salmonella enterica* serotype typhimurium SL1181 (Re mutant)	Sigma-Aldrich	Cat# L9516
Lipid A, monophosphoryl *Salmonella enterica* serotype minnesota Re 595 (Re mutant), Ready Made Solution	Sigma-Aldrich	Cat# SBR00012
Muramyldipeptide	InvivoGen	Cat# tlrl-mdp
Pam3CSK4	InvivoGen	Cat# tlrl-pms
Polymyxin B sulfate salt	Sigma-Aldrich	Cat# P4932-1MU
Recombinant DNA		
pcDNA3.1-FAM134B-WT-HA	Dikic Lab	N/A
pcDNA3.1-FAM134B-AHLmt-HA	This study	N/A
pcDNA3.1-FAM134B-AHCmt-HA	This study	N/A
pcDNA3.1-FAM134B-CTERmt-HA	This study	N/A
pcDNA3.1-FAM134B-DOUBLEmt1	This study	N/A
pcDNA3.1-FAM134B-DOUBLEmt2	This study	N/A
pcDNA3.1-FAM134B-TRIPLEmt	This study	N/A
pDEST-pMH-SFB-FAM134B	Dikic Lab	N/A
pGEX6P1-FAM134B-GST	Dikic Lab	N/A
Experimental Models: Cell Lines		
HeLa	ATCC	Cat# CCL-2; RRID: CVCL_0030
HEK293T	ATCC	Cat# CRL-3216; RRID: CVCL_0063
HeLa TREx Cells	Invitrogen	Cat# R71407; RRID:CVCL_D587
MEF WT	Christian Hübner	N/A
MEF FAM134BKO	Christian Hübner	N/A
BMDM WT	Christian Hübner	N/A
BMDM FAM134BKO	Christian Hübner	N/A
Experimental Models: Organisms/Strains		
Salmonella Typhimurium SL1344	Dikic Lab	N/A

Salmonella Typhimurium NCTC12023	Michael Hensel	N/A
Salmonella Typhimurium MvP887 (Δ*rfbP*)	Michael Hensel	N/A
Salmonella Typhimurium MvP886 (Δ*rfaL*)	Michael Hensel	N/A
Salmonella Typhimurium MvP885 (Δ*rfaG*)	Michael Hensel	N/A
Salmonella Typhimurium MvP759 (Δ*rfaH*)	Michael Hensel	N/A
Salmonella Typhimurium P3313 (*rfaL* complemented strain)	Michael Hensel	N/A
Salmonella Typhimurium P3314 (*rfaG* complemented strain)	Michael Hensel	N/A
Salmonella Typhimurium MvP2462 (Δ*ompA*)	Michael Hensel	N/A
Salmonella Typhimurium MvP2464 (Δ*tolAB*)	Michael Hensel	N/A
Salmonella Typhimurium MvP2555 (Δ*degS)*	Michael Hensel	N/A
Salmonella Typhimurium MvP544 (Δ*pagL)*	Michael Hensel	N/A
Enteropathogenic *Escherichia coli* O127:H6	Volkhard A. J. Kempf	N/A
Escherichia coli BL21	New England Biolabs	N/A
Escherichia coli Turbo	New England Biolabs	N/A
Software and Algorithms		
ClustalW	(Larkin et al., 2007)	https://www.ebi.ac.uk/Tools/msa/clustalw2/
iTOL server	(Letunic and Bork, 2021)	https://itol.embl.de/
GraphPad Prism 8.0	GraphPad Software	https://www.graphpad.com/
Zen (black edition)	Zeiss	https://www.micro-shop.zeiss.com/en/us/softwarefinder/software-categories/zen-black/
MaxQuant	(Tyanova et al., 2016a)	https://maxquant.net/maxquant/
Perseus	(Tyanova et al., 2016b)	https://maxquant.net/perseus/
Oligonucleotides (5' – 3 ')		
tolA Del13 For: GAGTAACAGGCGAACAGTTTTTTGGGAACCGAGAGTGTCAATTCCGGGGATCCGTCGACC-3'	This study	Michael Hensel
tolB Del13 Rev: TTCTTTAATTCCTTTAGTAATCAATTAATTATTATCACAGTGTAGGCTGGAGCTGCTTCG	This study	Michael Hensel
tolA DelCheck For:	This study	Michael Hensel

CGTTAGCGTCCATACCAGTG		
pagL Del For: AAATAACTATTGACATTGAAATGGTGGTGGAGTGTATATGGTGTAGGCTGGAGCTGCTTC	This study	Michael Hensel
pagL Del Rev: CTTCAGCCAGCAACTCGCTAATTGTTATTCAACTTCAGAACATATGAATATCCTCCTTAG	This study	Michael Hensel
pagL DelCheck For: GTGACATAACAGAAGTGTGG	This study	Michael Hensel
degS Del13 For: TGCTGCTGCCGTTCCCTTTTTTAACGACGCCTCCATCATGATTCCGGGGATCCGTCGACC	This study	Michael Hensel
degS Del13 Rev: CTAGTCGTCGAACGACGCGGGCAAAAGCCGCGTCGTTTTATGTAGGCTGGAGCTGCTTCG	This study	Michael Hensel
degS DelCheck For: GAAATGCGCAAAGTGATGGC	This study	Michael Hensel
ompA Del13 For: ATGGCGTATTTTGGATGATAACGAGGCGCAAAAAATGAAAATTCCGGGGATCCGTCGACC	This study	Michael Hensel
ompA Del13 Rev: CCCCGCGACGCGGGGTTTTTTATCAGACGGAAACTTAAGCTGTAGGCTGGAGCTGCTTCG	This study	Michael Hensel
ompA DelCheck For: AGCCGTAGATATCGGTAGAG	This study	Michael Hensel
K1 Red Del: CAGTCATAGCCGAATAGCCT	This study	Michael Hensel